Supplementary information:
Scaling sustainable aviation fuel for net-zero CO_2 emissions by 2050 – Pathways, requirements and challenges

Nils Bullerdiek*[a] (nils.bullerdiek@tuhh.de), Stefan Bube[a], Jelto Lange[a], Gunnar Quante[a], Steffen Voß[a], Martin Junginger[b], Martin Kaltschmitt[a]

[a] Hamburg University of Technology (TUHH), Institute of Environmental Technology and Energy Economics (IUE), Hamburg, Germany

[b] Utrecht University, Copernicus Institute of Sustainable Development, Utrecht, Netherlands

Table of Contents

1 SAF Deployment Linear Optimization Model

1.1 Mathematical Model Description

The following section provides a description of the linear optimization model based on [1] at the formalized (mathematical) level. The symbols, exponents, and indices used are presented in Section 1.2. The model is formulated as a linear optimization problem, with Equation (1.1) defining the objective function of the model.

$$c^{total} = \sum_{t \in T} \left[c_t^{KERO(F)} + c_t^{KERO(SAF)} + c_t^{OFFS} \right] (1+i)^{-t} \stackrel{!}{=} min \tag{1.1}$$

According to this objective function, the systemic total costs (system costs) for each year of analysis result from the use of conventional fossil kerosene, SAF kerosene, and carbon dioxide (CO_2) or GHG emissions offsetting. These annual costs are discounted to the most recent point before the actual analysis period (i.e., the reference year t_0). Following the overall model approach, i.e. aiming to integrate SAF kerosene into global aviation cost-efficiently (minimizing costs), the sum of the discounted values for all years of analysis is minimized. Within the model, monetary values are represented as real values adjusted for purchasing power, excluding potential inflation effects from consideration. The individual components of the objective function, along with the associated system of constraints within the model, are detailed in the following sections.

1.1.1 Fossil Kerosene

Equation (1.2) describes the system costs associated with the use of fossil kerosene.

$$c_t^{KERO(F)} = m_t^{KERO(F)} \left(p_t^{KERO(F)} + EF_t^{KERO(F)} p_t^{CO_2} \right) \quad t \in T \tag{1.2}$$

The annual costs associated with the use of fossil kerosene (*KERO(F)*) consist of two components: the costs of the kerosene quantity used, determined by the respective kerosene price (or procurement costs), and the costs of the carbon dioxide (CO_2) emissions resulting from kerosene use, calculated based on a specific CO_2 price.

1.1.2 SAF Kerosene

Equations (1.3) and (1.4) describe the systemic costs associated with the use of SAF kerosene options.

$$c_t^{KERO(SAF)} = \sum_{p\in P}\sum_{f\in F}\sum_{a\in A} m_{a,f,p,t}^{KERO(SAF)} \left(GK_{a,f,p,t}^{KERO(SAF)} + EF_{a,f,p,t}^{KERO(SAF)}\, p_t^{CO_2}\right) + \sum_{p\in P}\sum_{a\in A} A_{a,p,t}^{DCM}\; c_{a,p,t}^{DCM} \quad t \in T \quad (1.3)$$

$$m_{a,f,p,t}^{KERO(SAF)} = m_{a,f,p,t}^{HC}\, \omega_{a,p,t}^{KERO} \quad a \in A, f \in F, p \in P, t \in T \quad (1.4)$$

The systemic costs for the use of SAF kerosene in each year of analysis consist of three components. First, they include the quantities of the various kerosene options used and their specific production costs. Second, they account for the costs of the carbon dioxide (CO_2) emissions associated with kerosene use, calculated based on a specified CO_2 price. According to Equation (1.4), the production volume of SAF kerosene is derived from the hydrocarbon production volume of a conversion plant multiplied by the gravimetric share of the kerosene fraction. The third cost component includes the costs associated with decommissioning SAF production plants, which may arise if facilities need to be taken out of operation before reaching their assumed maximum technical operating lifetime.

1.1.3 SAF Production Plants

The modeling of fuel or hydrocarbon production, in conjunction with the required SAF production plant infrastructure, is carried out according to the Equations (constraints) (1.5) and (1.6).

$$\sum_{f\in F} m_{a,f,p,t}^{HC} \geq A_{a,p,t}^{STCK}\; PC_{a,p,t}^{HC}\, \rho_p^{min} \quad a \in A, p \in P, t \in T \quad (1.5)$$

$$\sum_{f\in F} m_{a,f,p,t}^{HC} \leq A_{a,p,t}^{STCK}\; PC_{a,p,t}^{HC}\, \rho_p^{max} \quad a \in A, p \in P, t \in T \quad (1.6)$$

According to the constraints outlined above, the hydrocarbon production volume is determined by the sum of facilities of a specific age and conversion process that utilize a defined resource category or multiple resource categories, along with their respective production capacities. The factors ρ_p^{min} and ρ_p^{max} define the facility utilization rate, representing the range of minimum and maximum utilization relative to production capacity. By summing over the resource category f, it

is ensured that the total volume of hydrocarbon products produced from different resource categories does not exceed the aggregate production capacity of the respective facilities within an age class a and conversion process p, on average.

Equations (constraints) (1.7) to (1.10) model the SAF production plant stock. For this purpose, a modeling approach based on [2] is applied. The SAF production facility stock is determined by the annual commissioning and decommissioning of SAF production plants over time.

$$A_{a,p,t}^{STCK} = A_{p,t}^{COM} \quad \text{für } a = 1 \quad a \in A, p \in P, t \in T \tag{1.7}$$

$$A_{a,p,t}^{STCK} = A_{a,p,t_1}^{ISTCK} + A_{a-1,p,t-1}^{STCK} - A_{a,p,t}^{DCM} \quad for\ a \geq 2 \quad a \in A, p \in P, t \in T \tag{1.8}$$

$$A_{a,p,t}^{DCM} = 0 \quad \text{für } a \leq n^{min} \quad a \in A, p \in P, t \in T \tag{1.9}$$

$$A_{a+1,p,t}^{DCM} = A_{a,p,t-1}^{STCK} \quad \text{für } a = n^{max} \quad for\ t \geq 2 \quad a \in A, p \in P, t \in T \tag{1.10}$$

The constraint described in Equation (1.7) adds SAF production plants that are being commissioned in a specific year of analysis to the SAF production plant stock. These plants are assigned an age of 1, referring to the end of the respective year. The constraint in Equation (1.8) then defines the SAF production plan stock for a given year. This stock is composed of an initial plant stock, exogenously specified as a parameter for the year t_1 (2025), and facilities from the previous year $(t-1)$ that are one year older $(a-1)$. Additionally, SAF production plants decommissioned at the beginning of the year are subtracted from the SAF production plant stock.

The constraint in Equation (1.9) ensures that a SAF production plant can only be decommissioned after reaching a specified minimum operational lifespan. Conversely, the constraint in Equation (1.10) mandates that a SAF production plant must be decommissioned no later than when it reaches its defined maximum operational lifespan. Decommissioned SAF production plants are assigned to the category of decommissioned plants and are subtracted from the SAF production plant stock according to Equation (1.8). In line with the constraints in Equations (1.5) and (1.6), decommissioned SAF production plants no longer contribute to the production of hydrocarbon products. Additionally, the constraint in Equation (1.11) restricts the pace of SAF production plant development over time.

$$\sum_{a \in A} A_{a,p,t}^{STCK}\, PC_{a,p,t} \leq f_p^{PC_{STCK}} \sum_{a \in A} A_{a-1,p,t-1}^{STCK}\, PC_{a-1,p,t-1} \quad for\ t > 1 \quad p \in P, t \in T \tag{1.11}$$

The constraint in Equation (6.11) establishes a dependency for the expansion of hydrocarbon production capacities on the installed production capacity of the previous year or years. Accordingly,

the installed production capacity of a conversion technology p over time can increase by a maximum of a defined multiple ($f_p^{PC_{STCK}}$) of the installed capacity from the preceding year. This ensures that the deployment of larger quantities of SAF kerosene in later years is only feasible in conjunction with a prior, gradual build-up of SAF production plants and production capacity. The modeling of production volumes for by-products (e.g., naphtha, diesel) is addressed through Equation (1.12).

$$m_{b,a,f,p,t}^{BP} = m_{a,f,p,t}^{HC}\, \omega_{b,a,p,t}^{BP} \quad b \in B, a \in A, f \in F, p \in P, t \in T \tag{1.12}$$

According to Equation (1.12), the volumes of by-products are derived from the total hydrocarbon production volume of the respective conversion facilities, taking into account the gravimetric share of the by-product fraction within a given conversion process. The gravimetric share of a by-product in the hydrocarbon production volume depends on the conversion process but is independent of the resource option used.

1.1.4 Feedstock Utilization

The constraints described in Equations (1.13) and (1.14) impose restrictions on resource utilization for hydrocarbon production over time.

$$\sum_{p\in P}\sum_{a\in A} m_{a,f,p,t}^{HC}\, \vartheta_{a,f,p,t}^{RES} \leq V_{f,t}^{RES} \quad f \in F, t \in T \tag{1.13}$$

$$\sum_{p\in P}\sum_{a\in A} m_{a,f,p,t}^{HC}\, \vartheta_{a,f,p,t}^{RES} \leq f_f^{RES} \sum_{p\in P}\sum_{a\in A} m_{a,f,p,t-1}^{HC}\, \vartheta_{a,f,p,t-1}^{RES} \quad for\ t > 1 \quad f \in F, t \in T \tag{1.14}$$

The constraint in Equation (1.13) ensures that the feedstocks used for hydrocarbon production (per feedstock category and year of analysis) do not exceed a defined feedstock availability. The resource demand for producing a specific volume of hydrocarbon products is calculated based on the mass- and energy-specific feedstock demand ($\vartheta_{a,f,p,t}^{RES}$).

The constraint in Equation (1.14) prevents the full utilization of a feedstock's availability in a single step. For each feedstock category, the feedstock usage in a given year is limited to a defined multiple (f_f^{RES}) of the feedstock usage from the previous year. This accounts for the fact that raw material supply – particularly for biomass-based SAF production plants and the associated biomass options – must be gradually developed and expanded (e.g., plantation establishment, devel-

opment of feedstock logistics systems). Additionally, this ensures that the introduction of a previously unused feedstock category into an existing production infrastructure requires a corresponding scale-up of feedstock supply systems.

For the use of CO_2 in PTL SAF kerosene production, point-source CO_2 from ATJ and FT-BTL SAF production sites is directly linked to the corresponding amounts of ATJ and FT-BTL SAF produced in the model. Specifically, the available CO_2 is tied to the quantities of hydrocarbon fuel products (e.g., naphtha, kerosene, diesel) generated through these conversion pathways. The respective modeling is detailed by Equation (1.15) and (1.16).

$$\sum_{a \in A} m^{HC}_{a,f,p,t} \; \vartheta^{RES}_{a,f,p,t} \; \leq + V^{PS\ CO2}_{t} \quad f = \{PS\ CO_2\}, p = \left\{PTL_{PS\ CO_2}\right\}, t \in T \tag{1.15}$$

$$V^{PS\ CO2}_{t} = \sum_{p=\{ATJ,FT-BTL\}} \sum_{f \in F} \sum_{a \in A} m^{HC}_{a,f,p,t} \; f^{PS\ CO2}_{f,p,t} \quad t \in T \tag{1.16}$$

The constraint in Equation (1.15) ensures that the annual CO_2 from point sources used as feedstock for hydrocarbon production in the Power-to-Liquid (PTL) point-source CO_2 pathway (across all plant ages) does not exceed the annually available point-source CO_2. Equation (1.16) defines the annual availability of point-source CO_2, which is determined by the CO_2 released during the production of hydrocarbon products (e.g., naphtha, kerosene, diesel) via the ATJ (alcoholic fermentation) and FT-BTL (water-gas shift, WGS) conversion pathways, based on the different feedstock categories used. This availability is calculated based on the quantity of hydrocarbon fuels produced by these pathways and a specific factor ($f^{PS\ CO2}_{f,p,t}$), which represents the quantity of CO_2 produced per unit of hydrocarbon fuel via the considered ATJ or FT-BTL pathway. The factor varies depending on the feedstock, the conversion pathway (ATJ or FT-BTL), and the analysis year.

1.1.5 CO_2 Emissions Offsetting

Equation (6.15) details the systemic costs associated with the use of carbon dioxide (CO_2) emissions offsetting. The systemic costs of carbon dioxide (CO_2) offsetting are calculated annually based on the offset quantity and the specific offset price. The constraints in Equation (1.18) to (1.21) place limits on the offsetting use.

$$c_t^{OFFS} = n_t^{OFFS}\, p_t^{OFFS} \quad t \in T \tag{1.17}$$

$$n_t^{OFFS} \leq m_t^{KERO_D}\, EF_t^{KERO(F)} - EM^{CNG} \quad t \in T \tag{1.18}$$

$$n_t^{OFFS} \leq m_{t-(t^{OFFS\_red}-t^{EM\_max\_red})}^{KERO_D}\, EF_{t-(t^{OFFS\_red}-t^{EM\_max\_red})}^{KERO(F)} - EM^{CNG} \;\; for\; t = t^{OFFS\_red} - t_0 \tag{1.19}$$

$$n_t^{OFFS} \leq n_{t-1}^{OFFS}\,(1 - r_t^{OFFS\_red}) \quad for\;\; t^{OFFS\_red} < t < t^{NZE} \tag{1.20}$$

$$n_t^{OFFS} \leq \sum_{p\in P}\sum_{f\in F}\sum_{a\in A} m_{a,f,p,t}^{KERO(SAF)}\; EF_{a,f,p,t}^{KERO(SAF)} \quad for\;\; t \geq t^{NZE} \tag{1.21}$$

The constraint in Equation (1.18) ensures that carbon dioxide (CO_2) offsetting is applied only to emissions exceeding a defined carbon-neutral growth (CNG) threshold (EM^{CNG}). This means CO_2 offsetting is used exclusively to maintain a CNG emission compliance (even if solely fossil kerosene is used to meet the kerosene demand), and not to achieve additional reductions in net CO_2 emissions.

The constraint in Equation (1.19) ensures that, starting from the year when the maximum allowable CO_2 offsetting usage is to be reduced (t^{OFFS_red}), such as 2040, the amount of CO_2 offsets utilized in that specific year is capped at the maximum level of CO_2 offsets that could have been used in the year ($t^{EM\_max\_red}$), such as 2035, when a reduction of the defined emission constraint (EM_t^{max}) could begin.

The constraint in Equation (1.20) ensures that, starting from the year when CO_2 offsetting usage is to be reduced (t^{OFFS_red}), such as 2040, and continuing until a definable net-zero CO_2 emissions target year (t^{NZE}), such as 2050, the annual amount of offsets utilized can decrease by a defined share ($r_t^{OFFS\_red}$).

The constraint in Equation (1.21) ensures that, starting from the defined net-zero CO_2 emissions target year (t^{NZE}), such as 2050, the annual amount of CO_2 offsets utilized cannot exceed the CO_2 emissions generated by using SAF kerosene. In other words, from that point onward, CO_2 offsetting is limited to compensating for emissions from SAF kerosene, and fossil kerosene emissions

can no longer be offset. Furthermore, if a net-zero CO_2 emissions level is set as the maximum allowable emissions from (t^{NZE}) onward, this also implies that the use of fossil kerosene would no longer be permitted.

1.1.6 Kerosene Demand and Emission Constraint

The constraint in Equation (1.22) models the fulfillment of a defined kerosene demand for each year.

$$m_t^{KERO(F)} + \sum_{p\in P}\sum_{f\in F}\sum_{a\in A} m_{a,f,p,t}^{KERO(SAF)} = m_t^{KERO_D} \quad t \in T \tag{1.22}$$

The specified kerosene demand can be met using both conventional fossil kerosene and SAF kerosene options. The total amount of SAF kerosene in a given year is calculated as the sum of kerosene quantities produced by SAF production plants across all age classes (a), feedstock categories (f), and conversion processes (p).

An emissions cap is implemented in the form of coherent carbon dioxide (CO_2) emission limits throughout the entire analysis period (emission cap trajectory). The model incorporates this requirement through the constraint defined in Equation (1.23).

$$m_t^{KERO(F)}\, EF_t^{KERO(F)} + \sum_{p\in P}\sum_{f\in F}\sum_{a\in A} m_{a,f,p,t}^{KERO(SAF)}\; EF_{a,f,p,t}^{KERO(SAF)} - n_t^{OFFS} \le EM_t^{max} \quad t \in T \tag{1.23}$$

This constraint ensures that the use of both fossil and SAF kerosene, combined with the respective carbon dioxide (CO_2) emissions offsetting, does not exceed the annually defined emission cap.

1.2 Symbols

The symbols, exponents, and indices used in the model are comprehensively listed in the following SI Table 1.

SI Table 1 Model Symbols, Exponents, and Indices

Symbol	Description
A_{a,p,t_1}^{ISTCK}	Number of initial SAF plants (initial plant stock (*ISTCK*)) of plants *A* with plant age *a*, conversion process *p* in year t_1
$A_{a,p,t}^{DCM}$	Number of decommissioned (*DCM*) plants *A* with plant age *a*, conversion process *p* in year *t* (decision variable)
$A_{a,p,t}^{STCK}$	Number / stock (*STCK*) of plants *A* with plant age *a*, conversion process *p* in year *t*
$A_{p,t}^{COM}$	Number of commissioned (*COM*) plants *A* with plant age *a*, conversion process *p* in year *t* (decision variable)
$EF_{a,f,p,t}^{KERO(SAF)}$	Specific CO_2 emission factor EF of SAF kerosene (*KERO(SAF)*) from plants with plant age *a*, feedstock category *f*, conversion process *p* in year *t*
$EF_t^{KERO(K)}$	Specific CO_2 emissions factor EF of fossil kerosene (*KERO(F)*) in year *t*
EM^{CNG}	Carbon-neutral growth (CNG) CO_2 emission threshold
EM_t^{max}	Maximum CO_2 emissions (emission constraint) EM in year *t*
$GK_{a,f,p,t}^{KERO(SAF)}$	Specific production costs GK of SAF kerosene option (*KERO(SAF)*) from plants with plant age *a*, feedstock category *f*, conversion process *p* in year *t*
$PC_{a,p,t}$	Plant specific production capacity (plant production output) PC of individual plants based on conversion process *p* with plant age *a* in year *t*
$PC_{a,p,t}^{HC}$	Plant specific production capacity (plant production output) PC of hydrocarbon(*HC*)-product (*HC*) of individual plants based on conversion process *p* with plant age *a* in year *t*
$V_{f,t}^{RES}$	Feedstock availability (*RES*) V of feedstock category f in year *t*
$V_t^{PS\,CO2}$	Point source CO_2 availability (*PS CO2*) V of in year *t*
$c_{a,p,t}^{DCM}$	Costs *c* of plant decommissioning (*DCM*) (before reaching maximum operating lifetime) for plants with plant age *a*, conversion process *p* in year *t*
$c_t^{KERO(F)}$	System costs *c* from usage of fossil kerosene (*KERO(F)*) in year *t*
$c_t^{KERO(SAF)}$	System costs *c* from usage of SAF kerosene (*KERO(SAF)*) in year *t*
c_t^{OFFS}	System costs *c* from CO_2 emissions offsetting (OFFS) in year *t*
c^{total}	Total (*total*) system costs *c* from usage of fossil kerosene ($KERO(F)$), SAF kerosene ($KERO(SAF)$) and CO_2 emissions offsetting ($OFFS$) across all analysis years *T*
$f_{f,p,t}^{PS\,CO2}$	Conversion factor f representing the specific quantity of usable point-source CO_2 per unit of hydrocarbon fuel product produced, based on the feedstock category f in conversion process *p* in year *t*
f_f^{RES}	Factor f for maximum expansion of usable feedstock quantities (*RES*) of feedstock category f
$f_p^{PC_{STCK}}$	Factor f for maximum expansion of installed production capacity (*PC*) of plant stock (*STCK*) for conversion process *p*
$m_{a,f,p,t}^{KERO(SAF)}$	Production quantity *m* of SAF kerosene (*KERO(SAF)*) from plants with plant age *a*, feedstock category *f*, conversion process *p* in year *t*
$m_{a,f,p,t}^{HC}$	Mass-quantity *m* of hydrocarbon(*HC*)-product of plant with plant age *a*, feedstock category *f*, conversion process *p* in year *t* (decision variable)
$m_{b,a,f,p,t}^{BP}$	Produced mass-quantity *m* of by-product (*BP*) *b* from plants with plant age *a*, feedstock category *f*, conversion process *p* in year *t*
$m_t^{KERO_D}$	Demand (*D*) of kerosene (*KERO*) *m* in year *t*
$m_t^{KERO(F)}$	Quantity *m* of fossil kerosene (*KERO(F)*) in year t (decision variable)
n^{max}	Maximum (*max*) operating lifetime *n* of a production plant
n^{min}	Minimum (*min*) operating lifetime *n* of a production plant
n_t^{OFFS}	Amount *n* an CO_2 emissions offsetting (OFFS) in year *t* (decision variable)

$p_t^{CO_2}$	Specific price p for carbon dioxide (CO_2) emissions in year t
$p_t^{KERO(F)}$	Specific price p of fossil kerosene (*KERO(F)*) in year t
p_t^{OFFS}	Specific price p for CO_2 emissions offsetting (OFFS) in year t
$r_t^{OFFS\_red}$	Share by which the annual amount of offsets utilized is decrease in year t
$t^{EM\_max\_red}$	Year when a reduction of the defined emission constraint (EM_t^{max}) begins
t^{NZE}	Net-zero CO_2 emissions target year
t^{OFFS_red}	Year when maximum allowable CO_2 offsetting usage is to be reduced
ρ_p^{max}	Maximum(*max*) utilization ρ of production plants with conversion process p
ρ_p^{min}	Minimum(*min*) utilization ρ of production plants with conversion process p
$\omega_{a,p,t}^{KERO}$	Gravimetric share ω of kerosene fraction (*KERO*) related to hydrocarbon production quantity from plants with plant age a, feedstock category f, conversion process p in year t
$\omega_{b,a,p,t}^{BP}$	Gravimetric share ω of by-product (*BP*) b an Kohlenwasserstoff-Produktionsmenge from plants with plant age a, feedstock category f, conversion process p in year t
$\vartheta_{a,f,p,t}^{RES}$	Mass- and energy-specific feedstock demand (RES) ϑ related to the total hydrocarbon fraction of a plant with plant age a, feedstock category f, conversion process p in year t
A	Set of plant ages (index a)
B	Set of by-products (index b)
F	Set of feedstock categories (index f)
P	Set of conversion processes (index p)
T	Set of analysis years (index t)
i	Discount rate

2 Description of SAF Conversion Technologies

2.1 Hydroprocessed Esters and Fatty Acids (HEFA)

The Hydroprocessed Esters and Fatty Acids (HEFA) conversion pathway involves the transformation of lipid-containing feedstocks into liquid hydrocarbons through catalytic hydrogenation, followed by cracking and isomerization of the intermediates [3], [4]. The corresponding HEFA conversion pathway is illustrated in SI Figure 1.

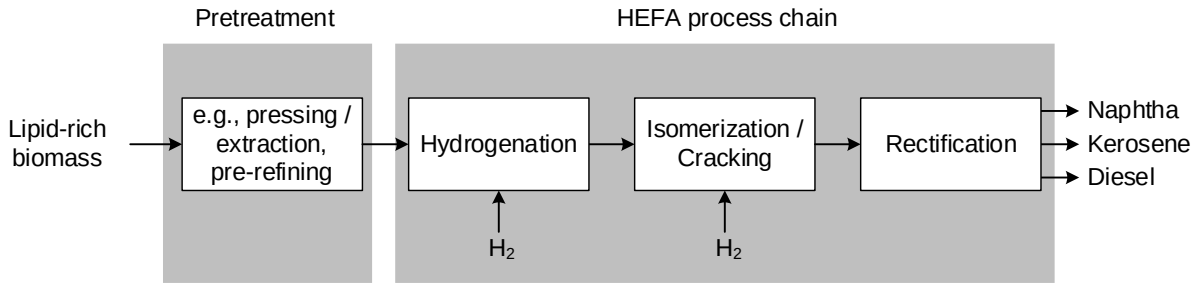

SI Figure 1 Schematic HEFA conversion pathway (**HEFA**: Hydroprocessed Esters and Fatty Acids)

Based on SI Figure 1, the HEFA conversion pathway is described in more detail below.

Supply of Oils and Fats

Practically all types of vegetable or animal oils and fats can be used as feedstock for the HEFA conversion pathway. From a purely technical perspective, this includes commonly traded "conventional" vegetable oils such as palm oil, soybean oil, or rapeseed oil, as well as other vegetable oils like those from Jatropha or Camelina plants and algal oils. Additionally, certain waste streams, such as used cooking oils or animal fats from slaughterhouses (e.g., animal tallow), can also serve as feedstock [5]. Depending on the raw material, specific pretreatment of the feedstock is required before the actual conversion process. These processes generally include, depending on the biogenic feedstock, size reduction, pressing and/or extraction processes, purification processes, and other pretreatment steps (e.g., degumming, neutralization) [6], [7].

HEFA Conversion Process Chain

The conversion of pretreated feedstocks takes place in two main transformation steps: hydrogenation or hydrotreatment, followed by isomerization and cracking. This is followed by product separation as the third process step.

Hydrogenation. In the first process step, a hydrogen treatment is carried out. During this step, the unsaturated double bonds of the triglycerides are saturated through the addition of hydrogen (H_2), and the glycerol backbone of the triglycerides is broken down with the formation of propane

(C_3H_8). Additionally, the oxygen (O) contained in the triglycerides is removed. Three possible reaction pathways can be used for this oxygen removal: hydrodeoxygenation (HDO), decarbonylation, and/or decarboxylation. Hydrodeoxygenation (HDO) is the preferred reaction for oxygen removal because it separates oxygen (O) in the form of water (H_2O) without any carbon loss. However, this reaction requires an adequate supply of hydrogen (H_2) [3], [6], [7], [8].[1]

In the case of complete hydrogenation, n-alkanes constitute the primary product of the hydrogenation process. Depending on the reaction used for oxygen removal, the carbon chain length of these n-alkanes either matches that of the fatty acids used as feedstock (in the case of hydrodeoxygenation, i.e., no carbon loss) or is shortened by one carbon atom compared to the profile of the original fatty acids (in the case of decarbonylation or decarboxylation) [3], [8].

Isomerization and Cracking. To produce kerosene as the desired end product, the n-alkanes resulting from hydrogenation must undergo further processing to meet the corresponding fuel requirements. This includes adjusting the carbon chain length to align with the carbon chain length range of the kerosene fraction. To achieve a high kerosene fraction, cracking of the n-alkanes is typically necessary [3], [9], [10]. Additionally, the low-temperature properties of the resulting product (n-alkanes) must be tailored to meet aviation fuel specifications, as n-alkanes generally have higher freezing points compared to branched alkanes (iso-alkanes) [6], [8]. Therefore, following hydrogenation, a cracking and isomerization step is usually performed in a dedicated reaction unit [3]. During this process, long-chain (unbranched) n-alkanes are catalytically converted into iso-alkanes (i.e., branched isomers) with the addition of hydrogen (H_2). These cracking processes typically occur in parallel with the isomerization processes [6], [8].

Product Separation. After any remaining gaseous components in the product stream (e.g., hydrogen (H_2), carbon monoxide (CO), carbon dioxide (CO_2)) [8], are separated from the liquid phase, the resulting product stream primarily consists of n- and iso-alkanes. This mass stream is then divided into the desired product fractions using standard rectification processes [6].

[1] Depending on the availability of hydrogen (H_2) for oxygen (O) removal, additional reactions typically occur alongside the HDO reaction. Decarboxylation generally takes place in parallel, while decarbonylation is less common. In decarbonylation, oxygen (O) is removed in the form of water (H_2O) and carbon monoxide (CO). In contrast, during decarboxylation, oxygen removal occurs exclusively in the form of carbon dioxide (CO_2) [6], [8], [9].

2.2 Alcohol-to-Jet (ATJ)

The Alcohol-to-Jet (ATJ) conversion pathway encompasses various process variants in which alcohols serve as the primary feedstocks and are transformed into a mixture of long-chain hydrocarbons (including those within the kerosene spectrum) through several sequential process steps [6]. This involves combining processes primarily known from refinery technology into a new integrated process [11]. The process chain can be divided into two main sections: alcohol production (1st step) and its subsequent conversion into hydrocarbon products (2nd step); this is illustrated in SI Figure 2 using ethanol as an example [12]. To date (as of March 2025), ethanol, isobutanol, and iso-butene have been approved as feedstocks; however, the approval of additional alcohol options (e.g., methanol, n-butanol) is being pursued [9], [13], [14].

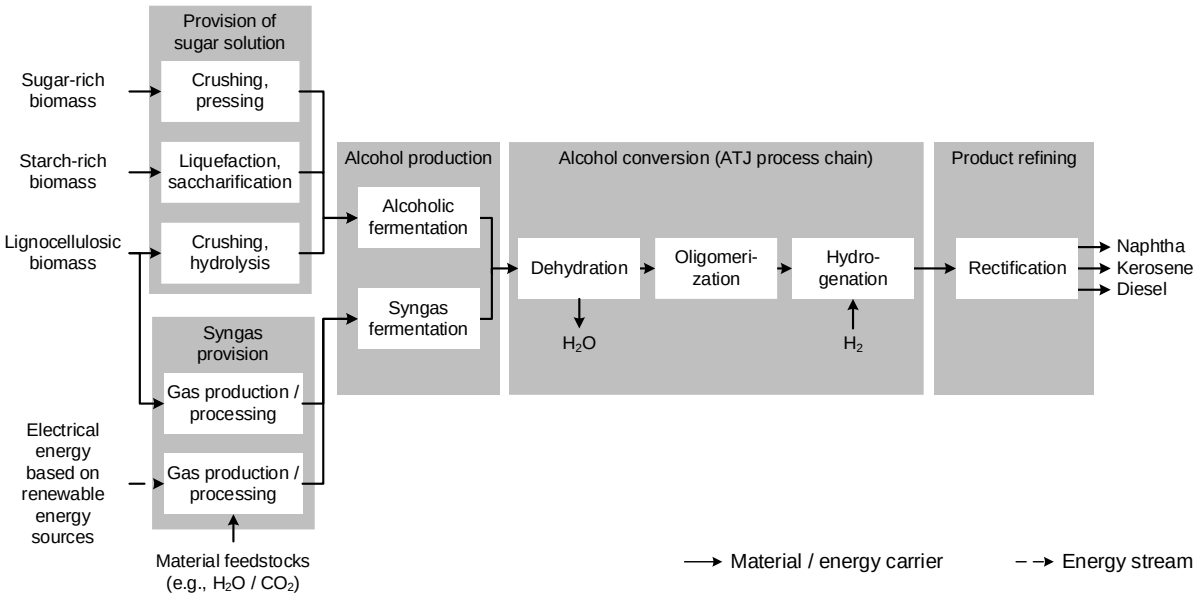

SI Figure 2 Schematic ATJ conversion pathway using ethanol as an example (**ATJ**: Alcohol-to-Jet)

Based on SI Figure 2, the Alcohol-to-Jet (ATJ) conversion pathway is described in more detail below using ethanol as a feedstock for conversion into higher hydrocarbons.

Alcohol Production

A variety of production pathways exist for the provision of ethanol (C_2H_5OH) [11], [15], [16], [17], [18], [19]. Below, the alcoholic (ethanol) fermentation and syngas fermentation processes are described in more detail.

- **Alcoholic Fermentation.** Alcoholic fermentation, or ethanol fermentation, is a biochemical process in which various microorganisms ferment a monosaccharide-based sugar solution under anaerobic conditions, primarily producing ethanol (C_2H_5OH) and carbon dioxide (CO_2). Yeasts are the preferred microorganisms, as they are relatively robust and easy to cultivate. Following the fermentation step, the ethanol (C_2H_5OH) contained in the fermented mash is

separated through multi-stage distillation or rectification and then concentrated (absolute ethanol production) [11], [20]. Essentially, sugar- and starch-rich biomasses are predominantly used as substrates today. Depending on the biomass used, various pretreatment steps are required to convert the sugar components in the biomass into a fermentable sugar solution [11], [21]. Sugar-rich biomass (e.g., sugarcane) is processed into a suitable solution with sufficient purity through simple pressing and/or washing, followed by cleaning steps. In the case of starch-rich biomass (e.g., corn), the sugar components embedded in the starch structure must first be released before fermentation can occur. This can be achieved, for example, by swelling or liquefying the starch, followed by saccharification [6], [21]. Due to its rigid cell structure, the utilization of lignocellulose also requires various pretreatment steps to convert it into a sugar solution for subsequent fermentation. Such processes are not yet commercially implemented. In corresponding pilot plants, this is typically done using two-stage methods. First, the lignocellulose matrix is broken down (e.g., via steam explosion), and the sugar molecules are then extracted from the cellulose and hemicellulose through enzymatic and/or acid-catalyzed hydrolysis [6], [22], [23].

- **Syngas Fermentation.** Various gas-fermenting microorganisms are capable of metabolizing gas components such as carbon monoxide (CO), carbon dioxide (CO_2), and/or hydrogen (H_2) [18]. Depending on the process conditions (e.g., aerobic or anaerobic conditions, syngas composition, microorganisms used), the syngas is converted in a biochemical fermentation step into products such as alcohols, acids, and other compounds [11], [18], [19]. Unlike thermochemical processes (e.g., Fischer-Tropsch synthesis), this conversion does not require a specific ratio of hydrogen (H_2) to carbon monoxide (CO) in the syngas. While gas cleaning steps are necessary, there is no need for gas conditioning to achieve optimal microbial activity [19]. The required syngas can be derived from a variety of biomass options or through electricity-based methods (Section 2.3 and 2.4).

Alcohol Conversion

The core Alcohol-to-Jet (ATJ) process section, i.e., the conversion of the alcohols used into long-chain hydrocarbons, involves the transformation steps of dehydration, oligomerization, and hydrogenation, followed by fractionation [24], [25], [26].

- **Dehydration.** During dehydration, oxygen (O) is removed from the hydroxyl group (OH) of the alcohol, resulting in the formation of water (H_2O). The alcohols used in this process primarily react to form short-chain alkenes (olefins). In the case of ethanol as the feedstock, a significant portion of these alkenes retains the same carbon chain length as the alcohol used [11], [27]; for example, when ethanol (C_2H_5OH) is used, a high proportion of ethylene molecules (C_2H_4) is produced.

- **Oligomerization.** The short-chain alkenes formed during dehydration are subsequently oligomerized, meaning they are "linked" into longer alkenes composed of structurally identical units. For example, multiple ethylene molecules (C_2H_4) are combined to form a new alkene with a longer carbon chain. This oligomerization – and thereby the composition of the final product fractions – is primarily influenced by pressure, temperature, residence time, and the choice of catalyst [6], [11].
- **Hydrogenation.** The oligomerized alkenes are hydrogenated at their carbon double bonds through the addition of hydrogen (H_2), resulting in their saturation. Similar to the dehydration and oligomerization steps, the hydrogenation process is catalytically supported [11].
- **Product Separation.** Following the above conversion steps, the produced hydrocarbon mixture is distilled into its various fractions. This typically involves rectification, a process commonly used in conventional refining. During rectification, the product fractions are separated based on their boiling points or boiling ranges (i.e., lighter fractions condense on the upper intermediate trays, while heavier fractions condense in the lower part of the rectification column) [11], [28].

Following this overall conversion pathway, the synthetic kerosene fraction produced is further refined to meet the specifications of aviation fuel [29].

2.3 Fischer-Tropsch-Biomass-to-Liquid (FT-BTL)

The Fischer-Tropsch (FT) conversion pathway involves the thermochemical transformation of synthesis gas (syngas) – composed of hydrogen and carbon monoxide – into synthetic crude oil (syncrude), which can be further processed into kerosene, among other products [30], [31]. The overall conversion consists of two main sections: syngas production and the subsequent Fischer-Tropsch synthesis, including the necessary product refining [32]. Syngas can be produced using a variety of combinations of feedstock options (based on renewable energy) and process variants, and it can be tailored for synthesis [6], [33], [34]. SI Figure 3 illustrates the corresponding overall Fischer-Tropsch-Biomass-to-Liquid (FT-BTL) pathway.

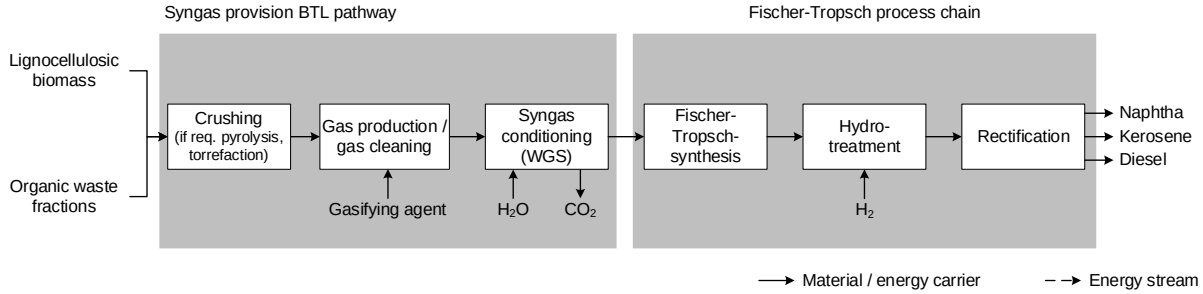

SI Figure 3 Schematic FT-BTL conversion pathway (**BTL**: Biomass-to-Liquid; **FT**: Fischer-Tropsch; **WGS**: water-gas shift)

Based on SI Figure 3, the Fischer-Tropsch-Biomass-to-Liquid (FT-BTL) conversion pathway is described in more detail below.

Syngas Provision

The Biomass-to-Liquid (BTL) conversion pathway, within the context of the Fischer-Tropsch conversion route, primarily involves the production of synthetic fuels through the thermochemical transformation of (typically) solid lignocellulosic biomass (e.g., straw, forest residual wood, short-rotation coppice) or solid organic waste fractions [6], [35]. This pathway is described below for the steps of feedstock pretreatment, gas production, and gas conditioning.

Feedstock Pretreatment. Depending on the feedstock and the logistical framework and boundary conditions, decentralized pretreatment of the feedstock at the site of raw material production or generation may be necessary. This could involve simple drying or more complex processes such as pyrolysis, torrefaction, or pelletization to, for example, increase the energy density of the transport material and potentially reduce transportation costs [5], [6]. As a result, the raw material catchment area and, consequently, the achievable feedstock input streams for a conversion plant can be expanded. This can facilitate the construction of larger plants and the utilization of cost-reduction effects through economies of scale [36], [37], [38], [39], [40], [41].

(Product-)Gas Production. During gas production (gasification), the macromolecules that make up the solid biomass feedstock are thermally decomposed under oxygen-deficient conditions [5].

The main components of the resulting product gas are carbon monoxide (CO), hydrogen (H_2), and carbon dioxide (CO_2). Depending on the process conditions, the gasifying agent used, or the reactor type (e.g., fixed-bed, fluidized-bed, or entrained-flow gasifiers), the proportions of individual gas components can vary significantly [6].

(Product-)Gas Conditioning. The produced syngas is subsequently conditioned to meet the requirements and conditions of the subsequent Fischer-Tropsch synthesis. This primarily involves product gas cleaning followed by gas conditioning.

The cleaning of the product gas (gas cleaning) involves processes such as the removal of particles, the elimination of tars, and/or the separation of inorganic gas components like sulfur or chlorine compounds [6]. The goal is to ensure that the produced syngas meets the purity requirements for the subsequent conversion process. This is particularly critical with respect to the catalysts used, as certain gas components can rapidly reduce their effectiveness (catalyst poisoning) [42], [43].

Before the cleaned raw syngas is fed into the Fischer-Tropsch reactor, the hydrogen (H_2) to carbon monoxide (CO) ratio in the syngas – referred to as the H_2-to-CO ratio – is adjusted during the conditioning process. For kerosene production, an H_2-to-CO ratio of approximately 2:1 is targeted [6], [30]. When gas is produced from solid biomass, the resulting product gas typically has a low H_2-to-CO ratio, indicating a hydrogen deficit [43], [44]. To adjust (i.e., increase) this ratio for the Fischer-Tropsch synthesis, the water-gas shift (WGS) reaction is employed. Steam (H_2O) is added to the syngas, allowing a portion of the carbon monoxide (CO) to oxidize into carbon dioxide (CO_2), releasing hydrogen (H_2) in the process. The carbon dioxide (CO_2) formed and present in the gas stream is subsequently removed. This step removes a portion of the carbon (C) originally contained in the biomass feedstock from the process chain, resulting in a carbon loss, as it is not converted into higher hydrocarbons [43], [44]. To achieve the final required H_2-to-CO ratio, the hydrogen-rich raw syngas produced in the water-gas shift reactor is then combined with the remaining cleaned product gas stream and mixed to create the necessary syngas composition [6].

Fischer-Tropsch Conversion Process Chain

Following the production or provision of syngas, the Fischer-Tropsch process chain is implemented.

Fischer-Tropsch Synthesis. In a Fischer-Tropsch synthesis, a variety of reactions occur, during which the hydrogen (H_2) and carbon monoxide (CO)-rich syngas is catalytically converted primarily into a synthetic crude oil. This is a complex multicomponent mixture of various hydrocarbon

compounds. The hydrocarbon mixture mainly consists of straight-chain or unbranched alkanes (n-alkanes) and alkenes, with hydrocarbon chain lengths ranging from methane (C_1) to solid waxes ($\geq C_{20}$) [30], [32], [43], [45]. The composition of the synthetic crude oil can be described by the so-called α-value, which represents the chain growth probability [30], [31]. This value depends on operating parameters such as pressure, temperature, and residence time, as well as the choice of catalyst and the H_2-to-CO ratio of the syngas [6], [30].

Product Refining (Hydrotreatment). Following the Fischer-Tropsch synthesis, the produced synthetic crude oil is first separated from the residual gas stream and then refined into the desired target products [46]. If kerosene is the desired main product, relatively high α-values of 0.9 are targeted. For this purpose, low-temperature Fischer-Tropsch processes are typically employed [6], [31], [43]. In this configuration, a larger portion of the synthetic crude oil's product distribution falls within the kerosene range compared to high-temperature Fischer-Tropsch processes. Another significant portion of the product lies in the diesel and wax range (i.e., products with longer carbon chains). To increase kerosene yield, this wax fraction is broken down into shorter-chain hydrocarbon products using cracking processes. Additionally, these products must be hydrogenated (i.e., saturated with hydrogen (H_2)) to meet aviation fuel specifications. This can be achieved either through explicit hydrogenation in dedicated hydrogenation reactors or through combined hydrogenation within the cracking process in so-called hydrocrackers[2] [6], [31], [32]. Parallel to the cracking processes, isomerization reactions also occur, during which a portion of the unbranched hydrocarbons is converted into branched hydrocarbons. To enhance product properties, particularly low-temperature performance, a separate (hydro)isomerization of the kerosene fraction can be conducted in addition to the isomerization within the cracking processes. The resulting mixture primarily consists of n-alkanes and iso-alkanes [6], [46].

Product Separation. Following the various aforementioned hydrogen (H_2) treatment steps (hydrotreatment), the resulting product spectrum is separated into individual fractions based on their boiling points or ranges using conventional rectification methods [30], [49].

[2] In hydrocracking, cracking processes and hydrogenation occur simultaneously [47]. It is a catalytic process in which the C-C bonds of long-chain hydrocarbons (primarily waxes) are broken. With the addition of hydrogen (H_2), these are converted into shorter-chain products such as naphtha, kerosene, or diesel. The added hydrogen (H_2) serves to saturate the free bonds of the resulting shorter-chain products [48], [17], [46].

2.4 Power-to-Liquid (PTL)

The Power-to-Liquid (PTL) conversion pathway, within the context of the Fischer-Tropsch (FT) and Methanol-to-Jet (MTJ) conversion routes (SI Figure 4), primarily involves the production of synthetic fuels based on syngas derived from water (H_2O) and carbon dioxide (CO_2) using ("renewable") electrical energy [33], [50]. These process chains are described below.

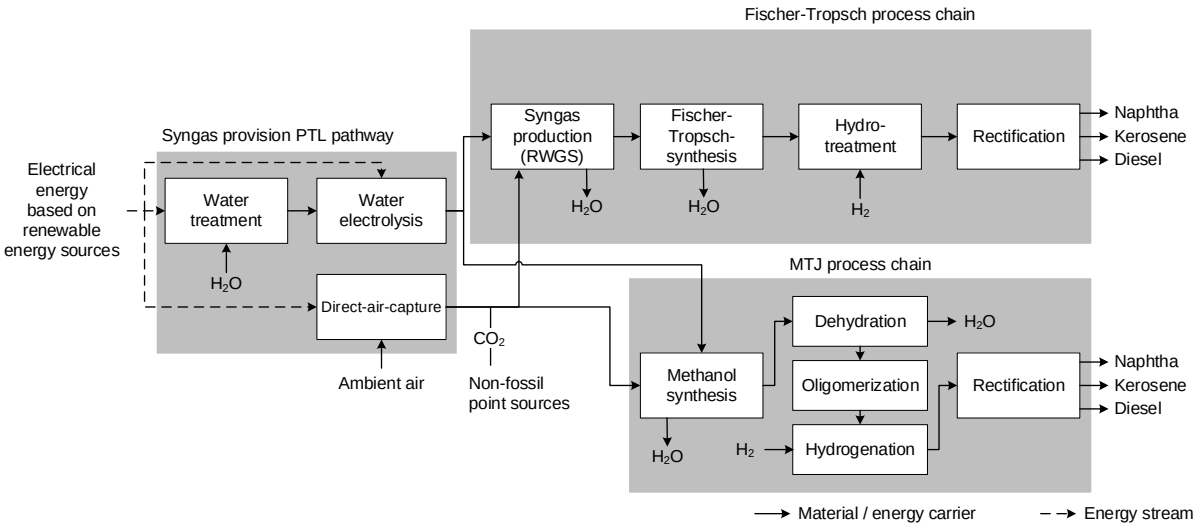

SI Figure 4 Schematic PTL conversion pathway with FT and MTJ process chains (**FT**: Fischer-Tropsch; **MTJ**: Methanol-to-Jet; **PTL**: Power-to-Liquid; **RWGS**: reverse water-gas shift)

Syngas Provision

Hydrogen (H_2) Provision. In the context of the Power-to-Liquid (PTL) conversion pathway, hydrogen (H_2) is typically produced using water (H_2O) as the feedstock [51]. Electrochemical water electrolysis is currently the most common method for splitting water. In this process, water (H_2O) is split into its components, hydrogen (H_2) and oxygen (O_2), in electrolyzers using electrical energy (direct current), without the formation of significant by-products or waste products [52], [53]. The main water electrolysis methods currently include alkaline water electrolysis (AEL), proton exchange membrane electrolysis (PEMEL), and solid oxide electrolysis (SOEL). On a larger industrial scale, only alkaline electrolysis (AEL) and proton exchange membrane electrolysis (PEMEL), both forms of low-temperature electrolysis, are currently in use. Solid oxide electrolyzers (SOEL), classified as high-temperature electrolysis, have so far only been demonstrated on a smaller scale [54], [55], [56], [57].

Carbon Dioxide (CO_2) Provision. In addition to hydrogen (H_2), carbon dioxide (CO_2) is the other main feedstock for syngas production in the Power-to-Liquid (PTL) conversion pathway. Two options for providing "renewable" carbon dioxide (CO_2) are distinguished below.

- **Provision from Point Sources (Byproduct or Combustion Product).** Carbon dioxide (CO_2) is generated as a byproduct in various biochemical (conversion) processes where biomass is

the primary feedstock. These processes primarily include biogas production and bioethanol production. Additionally, "renewable" carbon dioxide (CO_2) can be obtained as a combustion product of sustainably produced feedstocks. Examples include the combustion of wood (e.g., in (waste) wood incineration plants [58]) or the combustion of biomass- or electricity-based energy carriers (e.g., biomethane or "electricity-based" methane).

- **Direct-Air-Capture (DAC).** Ambient air, which is virtually available regardless of location and time, contains a small fraction of carbon dioxide (CO_2) at approximately 420 ppm or about 0.04 vol.%. This CO_2 can be "separated" using various capture technologies, such as adsorption, absorption, or membrane separation [56], [58], [59], [60]. Due to the large air or gas volumes that need to be processed relative to the separable amount of carbon dioxide (CO_2), many such processes are highly energy-intensive. For large-scale CO_2 capture from ambient air, absorption and adsorption processes are considered the preferred technologies [56], [58]. This technical capture of CO_2 from ambient air is often referred to as "Direct-air-capture" [59], [60].

After the provision of hydrogen (H_2) and carbon dioxide (CO_2), the subsequent steps diverge into the Fischer-Tropsch (FT) conversion process chain and the Methanol-to-Jet (MTJ) conversion process chain.

Fischer-Tropsch (FT) Conversion Process Chain

o produce syngas with a defined H_2-to-CO ratio for Fischer-Tropsch synthesis, the provided carbon dioxide (CO_2) must be converted into carbon monoxide (CO) [32]. This is achieved using the reverse water-gas shift (RWGS) reaction [61], which, compared to other technologies employed in this process, has not yet been implemented on a large industrial and commercial scale [57], [62]. In this process, hydrogen (H_2) and carbon dioxide (CO_2) are converted into water (H_2O) and carbon monoxide (CO) in a reactor operating at relatively high process temperatures (approximately 700 to 1,000 °C) [63], [64].

In addition to this method of syngas production, "co-electrolysis" can also be used to directly convert water (H_2O) and carbon dioxide (CO_2) into hydrogen (H_2) and carbon monoxide (CO). This can be achieved, for example, using solid oxide electrolyzers (SOECs) operated in co-electrolysis mode. In this approach, syngas with the required H_2-to-CO ratio is directly and immediately generated from the input feedstocks [31], [46], [55].

Following the production or provision of the required syngas, the subsequent steps of the Fischer-Tropsch process chain, as described in Section 2.3, are carried out.

Methanol-to-Jet (MTJ) Conversion Process Chain

The methanol pathway can be divided into two main process stages: "Methanol Production" and the subsequent "Methanol-to-Jet" (MTJ) conversion.

Methanol Production. Methanol synthesis involves a heterogeneously catalyzed process typically operated at temperatures of 200 to 300 °C and pressures ranging from 40 to 100 bar. The formation of methanol is described by specific reactions, with both reactions being interconnected through the water-gas shift (WGS) reaction, which occurs simultaneously. Due to the exothermic nature of the equilibrium-limited methanol formation reaction and its reduction in volume, the process benefits from lower temperatures and higher pressures. Compared to the traditional synthesis utilizing CO, the direct conversion of CO_2 achieves a significantly lower per-pass conversion rate (<45%) but demonstrates slightly higher selectivity (99.90–99.96%). The main by-products, such as ethanol, dimethyl ether, and methyl formate, are generated in minimal quantities [50].

Methanol-to-Jet (MTJ) process. The Methanol-to-Jet (MTJ) process, as illustrated in SI Figure 5, involves multiple steps. Notable commercial processes include the Mobil Olefins to Gasoline and Distillate (MOGD) process and the MtSynfuel process developed by Lurgi (now part of AirLiquide). However, these processes are not currently optimized specifically for kerosene production [50].

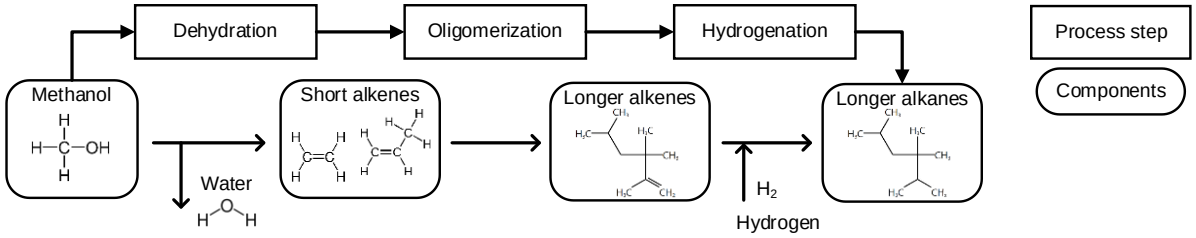

SI Figure 5 Schematic basic steps in MTJ conversion processes (based on [50] (Supplementary Information); **MTJ**: Methanol-to-Jet)

Similar to other alcohol-based conversion pathways (Alcohol-to-Jet, ATJ), the methanol-to-kerosene process involves olefin formation through dehydration, followed by oligomerization into higher olefins. Downstream hydrogenation then converts the unsaturated hydrocarbons into alkanes, which are finally separated into desired fuel fractions via distillation [50].

- **Dehydration.** Methanol dehydration to light olefins, known as the Methanol-to-Olefins (MtO) process, is a well-established technology (TRL 9). The process involves removing the hydroxyl group via water formation and creating a carbon-to-carbon double bond. Catalyst choice and operating conditions, such as pressure, temperature, and space velocity, influence the product distribution, with short-chain olefins being the primary output. Low temperatures and pressures favor the exothermic conversion, but methanol dehydration requires temperatures

above 350 °C and catalysts, such as protonated ZSM-5 and SAPO-34 zeolites, for complete conversion. Olefin selectivity ranges from 80 to 90% based on carbon input, with by-products including coke, short-chain olefins, and CO_2. Commercial MtO processes typically operate at around 400 °C and pressures below 5 bar, primarily producing ethene and propene as alternatives to naphtha cracking. For downstream oligomerization, higher carbon chain olefins, like butene or propene, are advantageous for producing hydrocarbons suitable for fuels. Shorter-chain olefins may yield a more uniform product with a smoother distillation curve, closely resembling conventional kerosene [50].

- **Oligomerization.** In the oligomerization process, carbon double bonds (C=C) in olefins (monomers) are broken and linked with other olefin molecules, forming C-C bonds and producing mono-unsaturated hydrocarbons (oligomers). This exothermic and volume-reducing reaction depends on the number of monomers and their carbon chain length. The technology used for oligomerization varies based on the reactant composition and target product, such as chain length and component type, with differences primarily determined by the catalyst employed. For kerosene production, acidic catalysts are crucial, as they also facilitate the formation of aromatics. Homogeneous transition-metal catalysts can also yield olefins suitable for kerosene. Depending on the MtO product, both single-stage and multi-stage processes are possible [50].
- **Hydrogenation and Fractionation.** Hydrogenation and fractionation of oligomerization products follow a process similar to that of Fischer-Tropsch (FT) crude. However, compared to FT crude, hydrogenation requires a greater amount of hydrogen (H_2) due to the input stream being a pure olefin mixture. Additionally, the hydrocarbons may pose greater challenges during hydrogenation as they tend to be more branched than the linear paraffinic (linear alkane) FT products. As in the FT pathway, in the MTJ pathway fractionation can be carried out using rectification [50].

3 Model Input-Data and Assumptions

SI Table 2 Full model input data (model data-input parameters for post-2050 are assumed to remain the same as in 2050; **ATJ**: Alcohol-to-Jet; **BM**: biomass; **BP/R**: by-products and residues; **BTL**: Biomass-to-Liquid; **DAC**: direct-air-capture; **EC**: energy crops; **FT**: Fischer-Tropsch; **HEFA**: Hydroprocessed Esters and Fatty Acids; **HC**: hydrocarbons; **PS:** point source; **PTL**: Power-to-Liquid)

Model-Input	Symbol	Unit	Year	Basecase	Progressive biofuel pathway	Conservative biofuel pathway	Progressive PTL pathway	Reference
FEEDSTOCK DATA								
Max. biomass availability for aviation	V^{RES}	EJ/a	2025–2050	30.0	60.0	15.0	≡ Basecase	SI Figure 7
– Lipid BP/R	V^{RES}	EJ/a	2025–2050	1.0	2.0	2.0	≡ Basecase	SI Figure 7
– Lipid EC	V^{RES}	EJ/a	2025–2050	2.0	4.0	4.0	≡ Basecase	SI Figure 7
– Stalky BP/R	V^{RES}	EJ/a	2025–2050	4.0	8.0	8.0	≡ Basecase	SI Figure 7
– Woody BP/R	V^{RES}	EJ/a	2025–2050	7.0	14.0	14.0	≡ Basecase	SI Figure 7
– Lignocellulosic EC	V^{RES}	EJ/a	2025–2050	11.0	22.0	22.0	≡ Basecase	SI Figure 7
– Organic waste	V^{RES}	EJ/a	2025–2050	5.0	10.0	10.0	≡ Basecase	SI Figure 7
Mass-/energy-specific feedstock demand								
– HEFA[a]	ϑ^{RES}	$GJ_{LIPID\ BM}/t_{HC}$	2025–2050	43	≡ Basecase	≡ Basecase	≡ Basecase	[6]
– ATJ (stalky BM)[a]	ϑ^{RES}	$GJ_{STALKY\ BM}/t_{HC}$	2025–2050	127	≡ Basecase	≡ Basecase	≡ Basecase	[6]
– FT-BTL (stalky BM)[a]	ϑ^{RES}	$GJ_{STALKY\ BM}/t_{HC}$	2025–2050	148	≡ Basecase	≡ Basecase	≡ Basecase	[6]
– FT-BTL (woody BM)[a]	ϑ^{RES}	$GJ_{WOODY\ BM}/t_{HC}$	2025–2050	96	≡ Basecase	≡ Basecase	≡ Basecase	[6]
– FT-BTL (organic waste)[a]	ϑ^{RES}	$GJ_{ORG\ WASTE}/t_{HC}$	2025–2050	101	≡ Basecase	≡ Basecase	≡ Basecase	[6]
– PTL (PS CO_2)	ϑ^{RES}	t_{CO2}/t_{HC}	2025–2050	3.45[b]	≡ Basecase	≡ Basecase	≡ Basecase	[65]
– PTL (PS CO_2)	ϑ^{RES}	GJ_{el}/t_{HC}	2025	90.8	≡ Basecase	≡ Basecase	≡ Basecase	[46], [66]
			2050	81.2	≡ Basecase	≡ Basecase	77.9	[46], [66]
– PTL (DAC CO_2)	ϑ^{RES}	GJ_{el}/t_{HC}	2025	109.4[c]	≡ Basecase	≡ Basecase	≡ Basecase [c]	[46], [66]
			2050	98.4[c]	≡ Basecase	≡ Basecase	94.2[c]	[46], [66]
Point source CO_2 availability ATJ/FT-BTL								

Model-Input	Symbol	Unit	Year	Basecase	Progressive biofuel pathway	Conservative biofuel pathway	Progressive PTL pathway	Reference
– ATJ (stalky BM)	$f^{PS\ CO2}$	t_{CO2}/t_{HC}	2025–2050	1.82[d]	≡ Basecase	≡ Basecase	≡ Basecase	-/-
– FT-BTL (stalky BM)	$f^{PS\ CO2}$	t_{CO2}/t_{HC}	2025–2050	4.11×0.80[e]	≡ Basecase	≡ Basecase	≡ Basecase	[6]
– FT-BTL (woody BM)	$f^{PS\ CO2}$	t_{CO2}/t_{HC}	2025–2050	5.01×0.80[e]	≡ Basecase	≡ Basecase	≡ Basecase	[6]
– FT-BTL (organic waste)	$f^{PS\ CO2}$	t_{CO2}/t_{HC}	2025–2050	5.01×0.80[e]	≡ Basecase	≡ Basecase	≡ Basecase	[6]
Factor for maximum expansion of usable feedstock quantities	f^{RES}	-	2025–2050	1,35[f]	≡ Basecase	≡ Basecase	≡ Basecase	-/-
SAF PRODUCTION PLANT DATA								
Initial plant stock[g]								
– HEFA	$A_{t_1}^{ISTCK}$	-	2025	5 (age 2) 4 (age 3) 3 (age 4) 2 (age 5) 1 (age 6)	≡ Basecase	≡ Basecase	≡ Basecase	[67], [68]
– ATJ	$A_{t_1}^{ISTCK}$	-	2025	1 (age 2)	≡ Basecase	≡ Basecase	≡ Basecase	[67], [68]
– FT-BTL (stalky BM), (woody BM), (organic waste)	$A_{t_1}^{ISTCK}$	-	2025	3 (age 2)	≡ Basecase	≡ Basecase	≡ Basecase	[67], [68]
– PTL (PS CO_2)	$A_{t_1}^{ISTCK}$	-	2025	1 (age 2)	≡ Basecase	≡ Basecase	≡ Basecase	[67], [68]
– PTL (DAC CO_2)	$A_{t_1}^{ISTCK}$	-	2025	1 (age 2)	≡ Basecase	≡ Basecase	≡ Basecase	[67], [68]
Plant production capacity[h]								
– HEFA	PC^{KWS}	kt_{HC}/a	2025/2050	500/1,000	≡ Basecase	500/500	≡ Basecase	SI Figure 8
– ATJ/FT-BTL	PC^{KWS}	kt_{HC}/a	2025/2050	100/200	≡ Basecase	100/100	≡ Basecase	SI Figure 8
– PTL	PC^{KWS}	kt_{HC}/a	2025/2050	100/200	≡ Basecase	≡ Basecase	100/500	SI Figure 8
Kerosene/by-product fractions								
– HEFA								
▫ Naphtha	ω^{BP}	%	2025–2050	25	≡ Basecase	≡ Basecase	≡ Basecase	[6]
▫ Kerosene	ω^{KERO}	%	2025–2050	65	≡ Basecase	≡ Basecase	≡ Basecase	
▫ Diesel	ω^{BP}	%	2025–2050	10	≡ Basecase	≡ Basecase	≡ Basecase	
– ATJ								
▫ Naphtha	ω^{BP}	%	2025–2050	10	≡ Basecase	≡ Basecase	≡ Basecase	[6]

Model-Input	Symbol	Unit	Year	Basecase	Progressive biofuel pathway	Conservative biofuel pathway	Progressive PTL pathway	Reference
▫ Kerosene	ω^{KERO}	%	2025–2050	80	≡ Basecase	≡ Basecase	≡ Basecase	
▫ Diesel	ω^{BP}	%	2025–2050	10	≡ Basecase	≡ Basecase	≡ Basecase	
– FT-BTL								
▫ Naphtha	ω^{BP}	%	2025–2050	15	≡ Basecase	≡ Basecase	≡ Basecase	[6]
▫ Kerosene	ω^{KERO}	%	2025–2050	80	≡ Basecase	≡ Basecase	≡ Basecase	
▫ Diesel	ω^{BP}	%	2025–2050	5	≡ Basecase	≡ Basecase	≡ Basecase	
– PTL								
▫ Naphtha	ω^{BP}	%	2025–2050	15	≡ Basecase	≡ Basecase	≡ Basecase	[46], [50]
▫ Kerosene	ω^{KERO}	%	2025–2050	80	≡ Basecase	≡ Basecase	≡ Basecase	
▫ Diesel	ω^{BP}	%	2025–2050	5	≡ Basecase	≡ Basecase	≡ Basecase	
Minimum plant utilization	ρ^{min}	-	2025–2050	1.00	≡ Basecase	≡ Basecase	≡ Basecase	-/-
Maximum plant utilization	ρ^{max}	-	2025–2050	1.00[i]	≡ Basecase	≡ Basecase	≡ Basecase	-/-
Minimum plant operating lifetime	n^{min}	Years	2025–2050	30	≡ Basecase	≡ Basecase	≡ Basecase	-/-
Maximum plant operating lifetime	n^{max}	Years	2025–2050	30	≡ Basecase	≡ Basecase	≡ Basecase	[6], [69], [70]
Factor for maximum expansion of installed production capacity	$f^{Pc_{STCK}}$	-	2025–2029	2.00[j]	≡ Basecase	≡ Basecase	≡ Basecase	SI Figure 9
			2030–2050	1.35	≡ Basecase	≡ Basecase	≡ Basecase	SI Figure 9
Plant decommissioning costs	c^{DCM}	€(2023)	2025–2050	0	≡ Basecase	≡ Basecase	≡ Basecase	-/-
KEROSENE FUEL DATA								
SAF kerosene								
– Specific CO_2 emissions factor	$EF^{KERO(\mathrm{SAF})}$	$kgCO_2eq/kg$	2025–2050	SI Figure 10, SI Figure 11	SI Figure 10, SI Figure 11	SI Figure 10, SI Figure 11	SI Figure 10, SI Figure 11	SI Figure 10, SI Figure 11
– Specific production costs	$GK^{KERO(\mathrm{SAF})}$	€(2023)/t	2025–2050	SI Figure 12, SI Figure 13	SI Figure 12, SI Figure 13	SI Figure 12, SI Figure 13	SI Figure 12, SI Figure 13	SI Figure 12, SI Figure 13
Fossil kerosene								
– Specific CO_2 emissions factor	$EF^{KERO(\mathrm{F})}$	$kgCO_2eq/kg$	2025–2050	3.97	≡ Basecase	≡ Basecase	≡ Basecase	[71]
– Specific price	$p^{KERO(\mathrm{F})}$	€(2023)/t	2025–2050	700	≡ Basecase	≡ Basecase	≡ Basecase	[72], [73], SI Figure 14

Model-Input	Symbol	Unit	Year	Basecase	Progressive biofuel pathway	Conservative biofuel pathway	Progressive PTL pathway	Reference
AIR TRANSPORT SYSTEM DATA								
Kerosene demand[k]	m^{KERO_D}	Mt/a	2025/2050	313/486	≡ Basecase	≡ Basecase	≡ Basecase	SI Figure 6
Max. net CO_2 emissions	EM^{max}	$MtCO_2eq$	2025–2035	1,146	≡ Basecase	≡ Basecase	≡ Basecase	SI Figure 6
	EM^{max}	$MtCO_2eq$	2050	0[l]	≡ Basecase	≡ Basecase	≡ Basecase	SI Figure 6
	$t^{EM\_max\_red}$	-/-	2035	2035	≡ Basecase	≡ Basecase	≡ Basecase	-/-
	t^{NZE}	-/-	2050	2050	≡ Basecase	≡ Basecase	≡ Basecase	-/-
	EM^{CNG}	$MtCO_2eq$	2025–2050	1,146	≡ Basecase	≡ Basecase	≡ Basecase	-/-
CO_2 emissions offsetting								
– Year of maximum allowable CO_2 offsetting usage reduction	t^{OFFS_red}	-	2040	2040	≡ Basecase	≡ Basecase	≡ Basecase	-/-
– Share of annual CO_2 offsetting reduction	$r_t^{OFFS\_red}$	%	2041–2050	5	≡ Basecase	≡ Basecase	≡ Basecase	-/-
– Specific CO_2 offsetting costs	p^{OFFS}	$€_{(2023)}/tCO_2eq$	2025	20	≡ Basecase	≡ Basecase	≡ Basecase	[74]
	p^{OFFS}	$€_{(2023)}/tCO_2eq$	2050	80[m]	≡ Basecase	≡ Basecase	≡ Basecase	[74]
Specific CO_2 emissions price (taxation)	p^{CO_2}	$€_{(2023)}/tCO_2eq$	2025–2050	0[n]	≡ Basecase	≡ Basecase	≡ Basecase	-/-
OTHER DATA								
Discount rate	i	-	2025–2050	0[o]	≡ Basecase	≡ Basecase	≡ Basecase	-/-

[a] The value applies to biomass-based plants, regardless of plant age or commissioning year; **[b]** The specific CO_2 demand from [65] was averaged for the Fischer-Tropsch (FT) and Methanol-to-Jet (MTJ) conversion pathways to provide an approximate representation of both of these pathways; **[c]** Refers to the commissioning year of the Power-to-Liquid (PTL) plant; **[d]** This factor is based on a stoichiometric coefficient for the biochemical conversion of sugar (sugar solution to ethanol) of 1.55 t_{CO2}/t_{EtOH} and the assumption of a subsequent conversion efficiency of downstream processes from ethanol to hydrocarbon products of 85%; **[e]** The CO_2 values from [6] were adjusted by a factor of 0.80 (i.e., only 80% considered) to account for potential losses during CO_2 recovery from the FT-BTL process. These losses include for example a carbon capture rate of approximately 90%, as well as additional inefficiencies due to challenges in using diffuse CO_2 sources (e.g., gas streams with low CO_2 concentrations) or further losses during purification and refinement; **[f]** Only considered for biomass options; For PTL plants, it is assumed that electricity is generated on-site (standalone/off-grid solution), with no external electricity supply. The annual biomass feedstock input can increase by a maximum of 35% per year, analogous to the assumed maximum capacity expansion of SAF conversion plants; **[g]** The initial SAF plant stock in the model is an approximation designed to ensure that the installed capacity for hydrocarbon fuel production, particularly SAF kerosene, aligns closely with estimates from the references, particularly [67]; **[h]** Linear yearly increase between 2025 and 2050; **[i]** For large-scale, continuously operated facilities, typical utilization rates range from 90% to 95% per year (7,884 to 8,322 full-load hours per year) [75]. For simplicity, in this analysis, an annual utilization rate of 100% (8,760 full-load hours per year) is assumed for all conversion facilities over the analysis period; **[j]** Applies only to ATJ, FT-BTL, and PTL plants; **[k]** The kerosene demand used in this analysis was calculated using the "Energy Demand Model," based on the methodology outlined by [1]. This model incorporates definable air traffic growth rates to represent various air transportation development scenarios. The calculated kerosene demand serves as input data for the optimization model used in the study; **[l]** Assumes a linear decrease between 2035 and 2050; **[m]** Assumes a linear increase between 2025 and 2050; **[n]** Potential regulatory mechanisms to promote SAF kerosene, such as CO_2 taxes, are not analyzed in depth in this study. Although the model can include a CO_2 tax on fossil and/or SAF kerosene, it was not applied during this analysis.; **[o]** The (real) discount rate considered here must be determined individually for each specific case analysis; the real discount rate for this analysis is set to zero, meaning no discounting is applied within the model. This approach aims to simplify the interpretation of systemic relationships by ensuring that input and output variables in the model are directly comprehensible.

3.1 Kerosene Demand and GHG Emissions Constraint

The following section outlines the development of kerosene demand and the emission constraints integrated into the SAF deployment linear optimization model, along with an explanation of how these variables were derived and defined.

Derivation of Kerosene Demand. The kerosene demand used as input data for the SAF deployment linear optimization model used in this analysis was derived using a model (or methodology) outlined by [1]. This model, referred to as the "Energy Demand Model" ("Energienachfragemodell"), is specifically designed to estimate possible energy demands – specifically kerosene demand – in international air transportation over a defined time horizon. The model is based on two primary input parameters of the commercial aviation system: the total transport performance of the global air transport system and the average transport efficiency of commercial aircraft systems (Commercial Aircraft System Fuel Efficiency, CASFE). These parameters form the foundation for estimating annual energy demand in aviation by aggregating the energy needs across all considered segments (e.g., passenger and freight air traffic). For each segment, the energy demand is further disaggregated by energy carrier option (e.g., kerosene or hydrogen, battery-electric). For a more detailed description of the model, refer to [1].

In applying this model ("Energy Demand Model"), kerosene was the only energy carrier considered for aviation. The transport performance levels for passenger and freight traffic in 2024 (t_0), based on data from [76], were used as a baseline and projected forward using varying air traffic growth rates, with annual fuel efficiency improvements factored into the projections. For the low air traffic growth scenario, annual transport performance growth rates of 2.0% for passenger traffic and 2.5% for freight traffic are assumed throughout the analysis period (here 2025 to 2055). In the medium air traffic growth scenario, annual growth rates are set at 3.0% for passenger traffic [77] and 3.5% for freight traffic [78]. In the high air traffic growth scenario, annual growth rates of 4.0% for passenger traffic and 4.5% for freight traffic are assumed. Across all growth scenarios, a fixed annual improvement in transport fuel efficiency of 1.3% for both passenger and freight segments is applied over the entire analysis period (here 2025 to 2055) [79]. The resulting kerosene demand estimated using this model ("Energy Demand Model") is presented in SI Figure 6 for the three different air traffic growth pathways.

Definition of GHG Emission Constraint. To align with the objectives of this analysis, a net-zero carbon dioxide (CO_2) emissions target is assumed for 2050. Furthermore, the aviation industry has committed to achieving carbon-neutral growth from 2020 onward, meaning the sector's net CO_2 emissions are to remain at 2019 levels starting from 2020 [80], [81]. Beyond these targets, no additional specifications currently exist, such as decade-specific emissions goals. To establish a suitable emissions reduction pathway (emission constraint) over time for this analysis, existing

scenarios and studies from the aviation industry are used as references [77], [82]. Based on these, the net CO_2 emissions level of global commercial aviation in 2019 is defined as the maximum allowable emissions level through 2035. Afterward, annual emissions caps decline linearly, reaching net-zero CO_2 emissions by 2050. The resulting emission constraint applied in this analysis for all air traffic growth pathways using the SAF deployment linear optimization model is illustrated in SI Figure 6.

Kerosene Demand and Emission Constraint in this Analysis. This section outlines the development of kerosene demand and the emission constraints incorporated into the SAF deployment linear optimization model. SI Figure 6 illustrates the kerosene demand trends for the three aviation growth scenarios considered in this study. It also shows the emission constraint applied in the model, along with the historical (2005 to 2024) kerosene consumption of global commercial aviation.

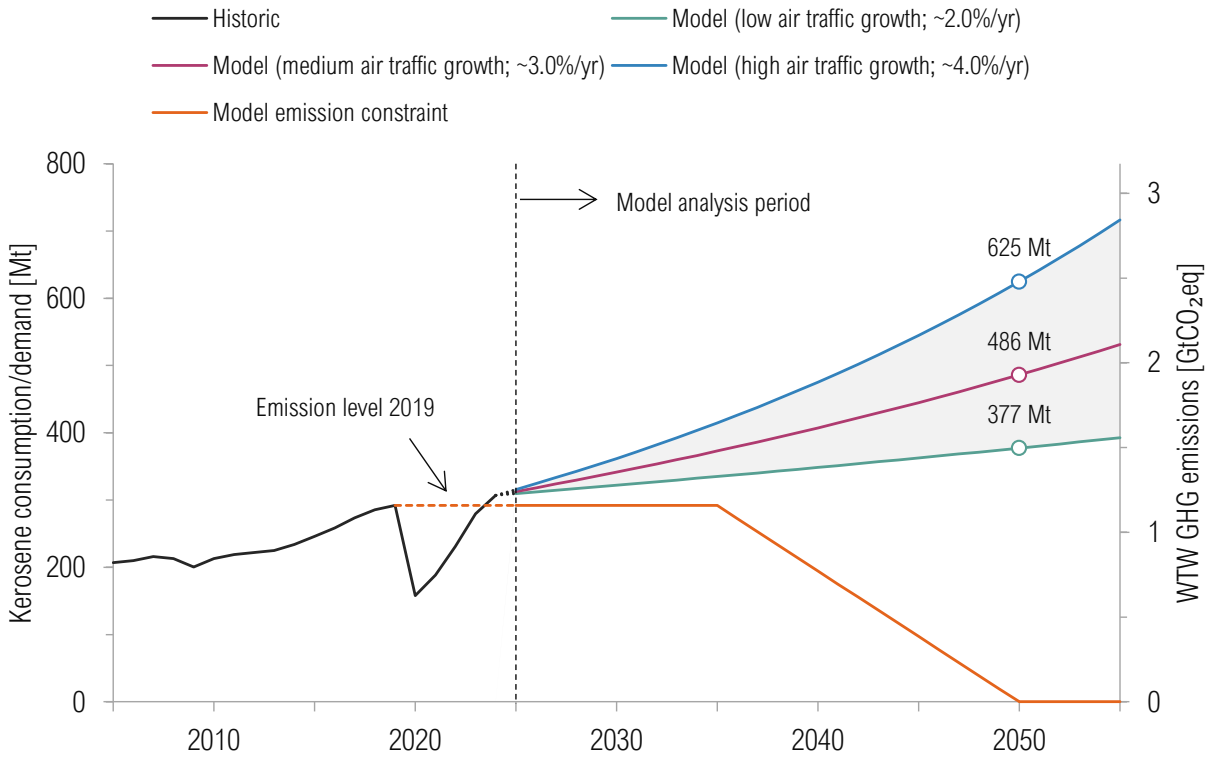

SI Figure 6 Kerosene demand and emission constraint considered in this analysis (**WTW**: Well-to-Wake; emission constraint trajectory based on [77]; historical kerosene consumption data from [76], [83], [84], [85], [86], [87], [88], [89], [90])

Based on SI Figure 6, kerosene demand increases steadily throughout the analysis period across all air traffic growth scenarios considered (low, medium, and high). In the low air traffic growth scenario, kerosene demand rises from approximately 310 Mt in 2025 to around 377 Mt in 2050, reflecting a total growth factor of about 1.2 and an average annual increase of about 0.8%. Similarly, in the medium air traffic growth scenario, demand grows from about 294 Mt in 2025 to ap-

proximately 465 Mt in 2050, corresponding to a total growth factor of about 1.6 and a yearly increase of about 1.8%. In the high air traffic growth scenario, demand increases from roughly 316 Mt in 2025 to around 625 Mt in 2050, with a total growth factor of about 2.0 and an annual increase of about 2.8%.

These increases in kerosene demand illustrate that the assumed improvements in fuel efficiency for commercial aircraft systems over time are overcompensated by the assumed air traffic growth in air transport performance. To maintain net CO_2 emissions at 2019 levels through 2035, an emissions cap of approximately 1,146 $MtCO_2eq$ is implemented. After 2035, emissions are reduced linearly, reaching net-zero CO_2 emissions by 2050. This creates a progressively stricter need for CO_2 emissions reductions, especially after 2035, as the emissions caps decrease while kerosene demand continues to increase.

3.2 Biomass Feedstock Availability

The biomass resources potentials that can actually be utilized in reality are determined – depending on the specific potential considered (e.g., technical, economic, or sustainably usable potential)[3] – by a combination of various framework conditions and boundary parameters [91], [93], [94], the future development of which is inherently unknown. In relevant biomass potential/availability assessments, a multitude of different assumptions are necessarily made regarding such and other influencing factors. Therefore, an accurate determination of biomass resource potentials is not reliably feasible; corresponding estimations are always associated with (sometimes significant) inaccuracies and, in some cases, very wide ranges of uncertainty [95], [96].

Given these uncertainties, different biomass availabilities are considered in the various study scenarios, based on literature-based potential assessments. SI Figure 7 illustrates a range of estimates for the global potentials or the global availability of sustainable biomass (left) and the relative shares of the different biomass options (right). Also shown are the biomass availabilities aligned with these estimates for each study scenario (for the year 2050); these are described in more detail below.

[3] For an explanation of various potential terms (e.g., theoretical, technical, economic, and sustainable (usable) potential), see [91], [92].

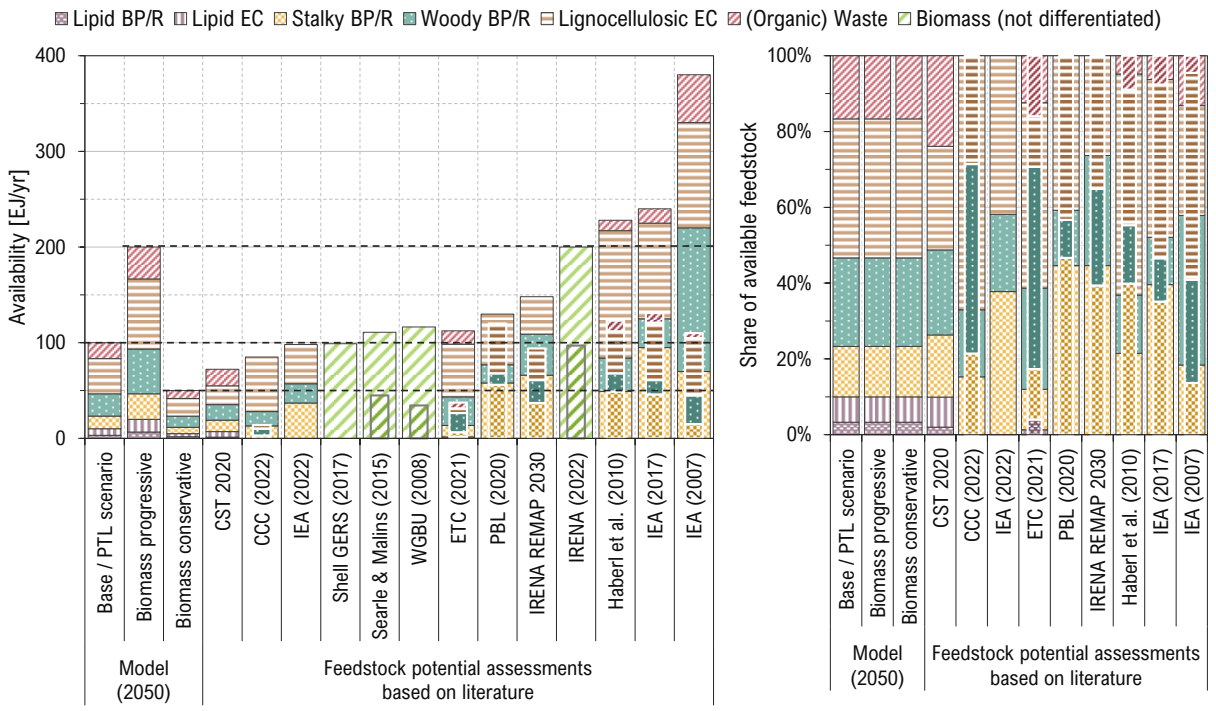

SI Figure 7 Scenario-specific biomass availability (2050) and classification in literature based data (**BP/R**: by-products and residues; **EC**: energy crops; **PTL**: Power-to-Liquid; the inner/front columns represent lower estimates, while the outer/rear columns indicate upper estimates. Potential estimates are derived from sources [35], [93], [94], [95], [97], [98], [99], [100], [101], [102], [103], [104], which present varying potential values depending on the study, reflecting technical, economic, and sustainably usable potentials (primarily economic/sustainable))

The estimates of globally available sustainable biomass depicted in SI Figure 7 (left) mostly range between approximately 100 and 250 EJ/a. For the basecase and the progressive PtL pathway scenario, an annual biomass availability of 100 EJ/a is considered, aligned with estimates across the entire range of global biomass availabilities shown in SI Figure 1; this value lies roughly in the midrange of the potential estimates depicted in SI Figure 7. Building on this, the progressive biomass scenario (progressive biofuel pathway) assumes a higher biomass availability corresponding to the scenario's orientation; here, a biomass availability twice that of the base scenario (200 EJ/a) is assumed, aligned with the upper range of potential estimates in SI Figure 7. Similarly, the conservative biomass scenario (conservative biofuel pathway) examines a biomass availability half that of the base scenario (approximately 50 EJ/a), which aligns with the lower range of the potential estimates shown in SI Figure 7.

Furthermore, the globally available biomass will likely not be exclusively available for the aviation sector in the future; other sectors and applications are also expected to demand biomass (or carbon), particularly for material uses (e.g., the wood-processing industry, construction materials industry, bio-plastics industry). To account for such aspects, it is simplistically assumed that at most 30% of the available biomass, or of each individual biomass category (e.g., lignocellulosic energy crops), can be allocated for use in the aviation sector.

Furthermore, in all scenarios, it is assumed that the lignocellulosic energy crops will be used up to a maximum of half (50%) in the form of stalky biomass or woody biomass until the respective overall availability of lignocellulosic energy crops is reached. This ensures a diversified use of stalky and woody biomass within this biomass feedstock option.

3.3 Plant Production Capacity

The production capacity of a SAF kerosene plant typically depends on various factors that can vary on a case-by-case basis, such as centralized or decentralized plant design, local feedstock availability, and technological maturity. As a reference, SI Figure 8 illustrates the distribution of production capacities for existing and planned SAF kerosene plants (as of May 2023), based on data from [68]. The model input data for plant sizes (production capacities) is based on the dataset shown in SI Figure 8 and supplemented with additional sources [105], [106], [107], [108].

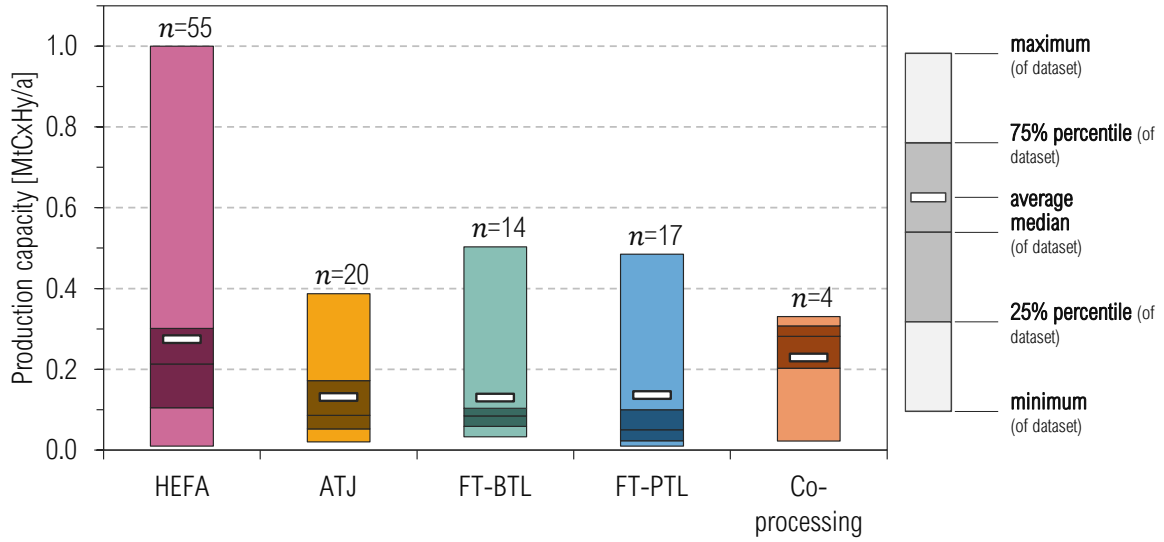

SI Figure 8 Overview of production capacities for existing and planned facilities for SAF kerosene production as of May 2023 (**ATJ**: Alcohol-to-Jet; **BTL**: Biomass-to-Liquid; **CxHy**: hydrocarbons; **FT**: Fischer-Tropsch; **HEFA**: Hydroprocessed Esters and Fatty Acids; ***n***: sample size; **PTL**: Power-to-Liquid; data based on May 2023 figures from [68])

3.4 Yearly Scaling of SAF Production Plant Capacity

In the modeling of the linear optimization model used here, the expansion of installed production capacity for a specific SAF conversion technology occurs incrementally within defined limits. For any given year, the capacity increase can be at most a (definable) multiple ($f^{PC_{STCK}}$) of the installed production capacity from the previous year (Section 1.1; Equation (1.11)). The model input-data used for this is based on the historical expansion trends of global photovoltaic and wind power plants, although such a comparison with these technologies is only partially applicable. These trends are illustrated in SI Figure 9.

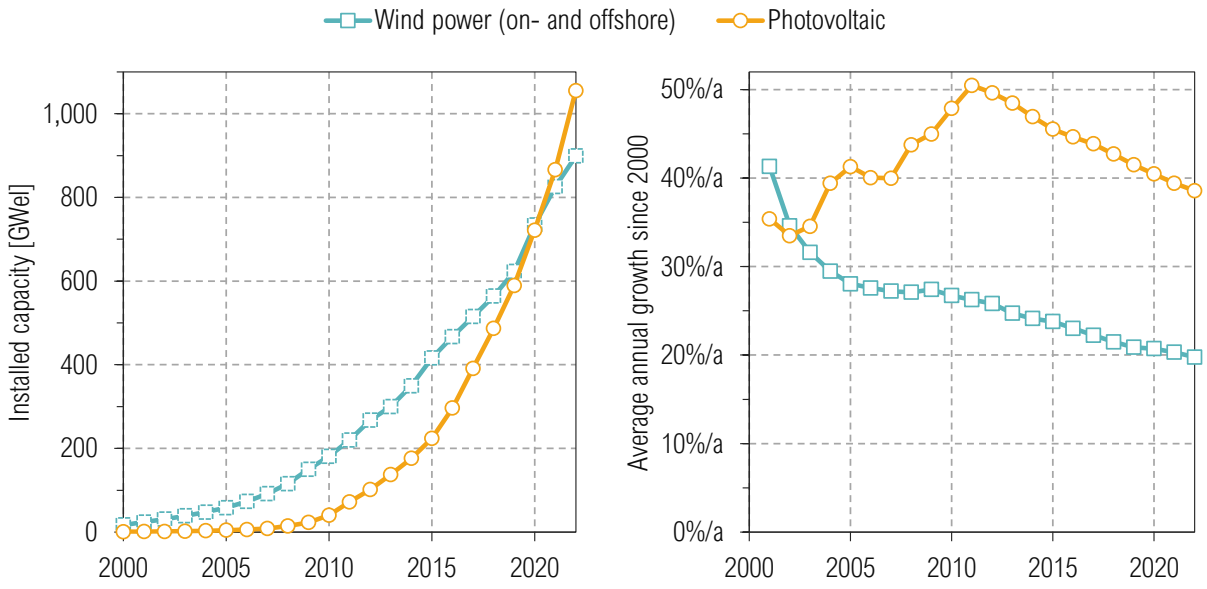

SI Figure 9 Development of installed capacity and growth rates of global photovoltaic and wind power plants between 2000 and 2022 (data based on [109])

According to SI Figure 9 , the average annual growth of globally installed photovoltaic capacity between 2000 and 2022 was approximately 40% per year, while wind power capacity grew by around 20% per year. Based on these figures, and to define the model solution space without overly constraining it, a maximum annual increase in installed production capacity of 35% per year ($f^{PC_{STCK}}$=1.35) is assumed for each conversion pathway. For conversion pathways that are less technologically advanced from today's perspective – specifically the ATJ, FT-BTL, and PTL options – a higher initial growth rate is allowed. It is assumed that the installed production capacity for these options can double ($f^{PC_{STCK}}$ = 2) during the first five years of the analysis period (2025 to 2029).

3.5 SAF Kerosene CO_2 Emissions and Production Costs

The following section details the specific CO_2 emissions and production costs of the SAF options included in this analysis within the SAF deployment linear optimization model, along with an explanation of how these values and parameters were determined and defined.

Derivation of SAF CO_2 Emissions and Production Costs. The specific CO_2 emissions and production costs for the SAF options considered in this analysis, used as input data for the SAF deployment linear optimization model, were calculated using the methodology outlined in [1]. Referred to as the "SAF Conversion Plant Model", this approach is designed to model and compute the specific CO_2 emissions and kerosene production costs for variable combinations of feedstock options and SAF conversion pathways. The model is a time-discrete, eco-economic calculation framework built on the principles of life cycle assessment (LCA) and dynamic cost-benefit analysis. For a detailed description of the entire model, refer to [1].

The model is based, among other factors, on specific material and energy input streams – i.e., the specific demands for primary feedstocks, auxiliary materials, and electrical energy needed to produce a defined quantity of hydrocarbon products. These specific input streams form the basis for the material and energy flow balance of a certain SAF conversion pathway (SAF option). From the calculated hydrocarbon production volume and the resulting product fractions, the quantities of kerosene and other by-products (e.g., naphtha, diesel) can be derived.

SAF Carbon Dioxide (CO_2) Emissions. Based on the material and energy flow balances, a life cycle assessment (LCA) is performed within the "SAF Conversion Plant Model". The analysis focuses exclusively on the anthropogenic greenhouse effect (GWP 100) as the environmental impact category. The results, and thus the corresponding model output values, are expressed in carbon dioxide (CO_2) equivalents per ton of kerosene (tCO_2eq/t). The assessment includes the environmental impacts of the material and energy input streams, accounting for the upstream processes or supply chains (e.g., raw material production and transportation) up to the point of delivery to the conversion plant. However, CO_2 emissions from fuel combustion in aircraft turbines are excluded, as the carbon released during combustion is assumed to have been previously removed from the atmosphere through biological and/or technical processes, maintaining a closed carbon cycle. Environmental impacts are allocated to unavoidable by-products based on their proportional energy content within the total hydrocarbon production volume, calculated using lower heating values. For a detailed explanation of the entire model, refer to [1].

SAF Production Costs. The modeling of specific SAF kerosene production costs, like the life cycle assessment, is based on the material and energy flow balances within the "SAF Conversion Plant Model". These costs are calculated through an annual accounting of capital-related, consumption-related, operational, and other expenses, as well as revenues from by-product sales. The total costs are then allocated to the kerosene production volume based on the energy content of the total hydrocarbon output, measured by lower heating values. Capital-related costs are modeled by estimating the specific investments for individual components of a conversion plant and converting these into annually constant cash flows using the annuity method. Consumption-related costs are calculated based on assumed prices or procurement costs for the various input streams (e.g., biomass feedstocks). Additionally, operational and other costs are determined in relation to the total investment of the respective conversion plant. For a detailed explanation of the entire model, refer to [1].

SAF CO_2 Emissions in this Analysis. The specific CO_2 emissions of the SAF kerosene options analyzed in this study, as estimated using the "Conversion Plant Model", are presented in the following figures. SI Figure 10 illustrates the specific CO_2 emissions of the SAF options, while SI Figure

190 11 provides these emissions for the basecase scenario alongside literature data for additional con-
191 text and comparison.

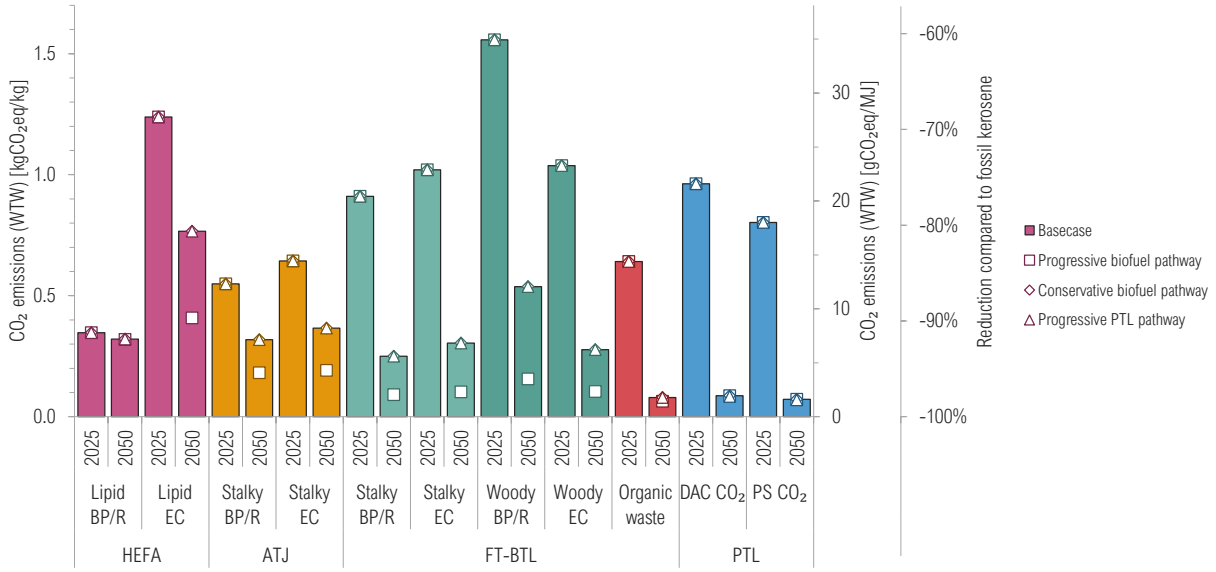

192

193 SI Figure 10 Carbon dioxide (CO_2) emissions of SAF kerosene options for plant commissioning years
194 2025 and 2050 across all scenarios (**ATJ**: Alcohol-to-Jet; **BP/R**: by-products and residues;
195 **BTL**: Biomass-to-Liquid; **DAC**: direct-air-capture; **EC**: energy crops; **FT**: Fischer-Tropsch;
196 **HEFA**: Hydroprocessed Esters and Fatty Acids; **PS:** point source; **PTL**: Power-to-Liquid;
197 **WTW**: well-to-wake; reduction compared to fossil kerosene based on specific CO_2 emissions
198 of 3.97 $kgCO_2eq/kg$ [71])

199

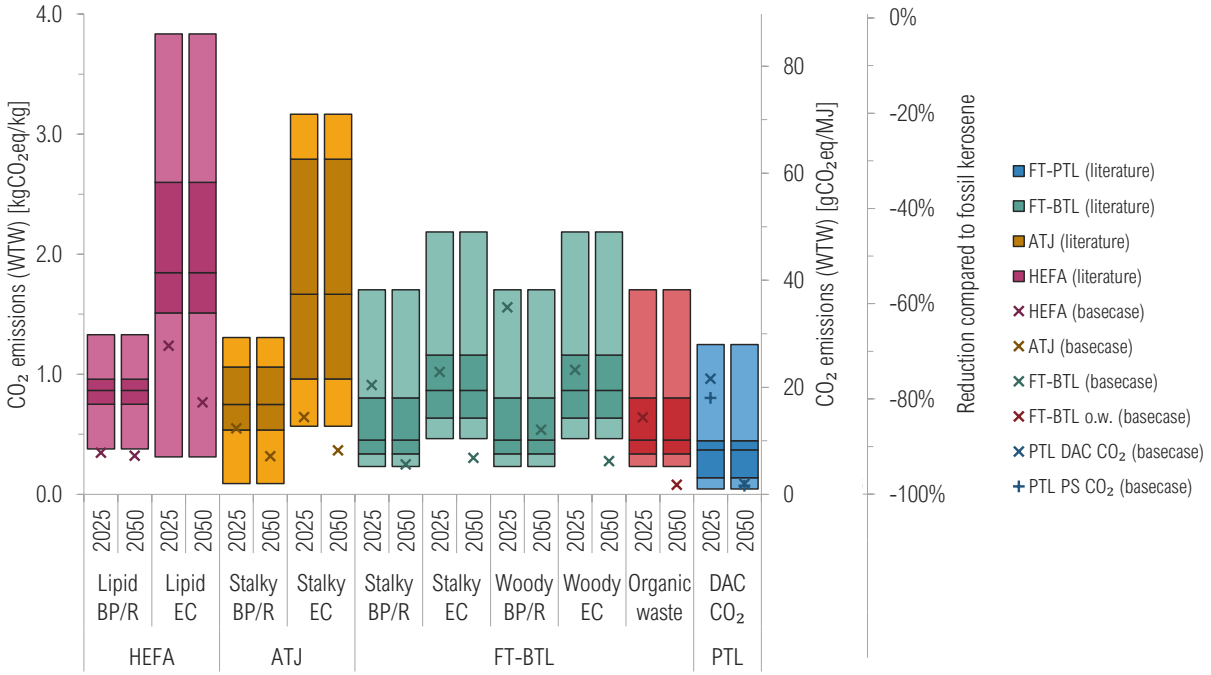

SI Figure 11 Carbon dioxide (CO_2) emissions of SAF kerosene options for plant commissioning years 2025 and 2050, presented for the basecase scenario and compared with literature data (**ATJ**: Alcohol-to-Jet; **BP/R**: by-products and residues; **BTL**: Biomass-to-Liquid; **DAC**: direct-air-capture; **EC**: energy crops; **FT**: Fischer-Tropsch; **HEFA**: Hydroprocessed Esters and Fatty Acids; **PS:** point source; **PTL**: Power-to-Liquid; **WTW**: well-to-wake; reduction compared to fossil kerosene based on specific CO_2 emissions of 3.97 $kgCO_2eq/kg$ [71]; for the literature values, no distinction is made here between the years 2025 and 2050 shown; literature data for ATJ, FT-BTL, HEFA based on [3], [70], [110], [111], [112], [113], [114], [115], [116], [117], [118], [119], [120]; literature data for PTL based on [33], [111], [121])

SAF Production Costs in this Analysis. The specific production costs of the SAF kerosene options analyzed in this study, as estimated using the "Conversion Plant Model", are presented in the following figures. SI Figure 12 illustrates the specific CO_2 emissions of the SAF options, while SI Figure 13 provides these emissions for the basecase scenario alongside literature data for additional context and comparison.

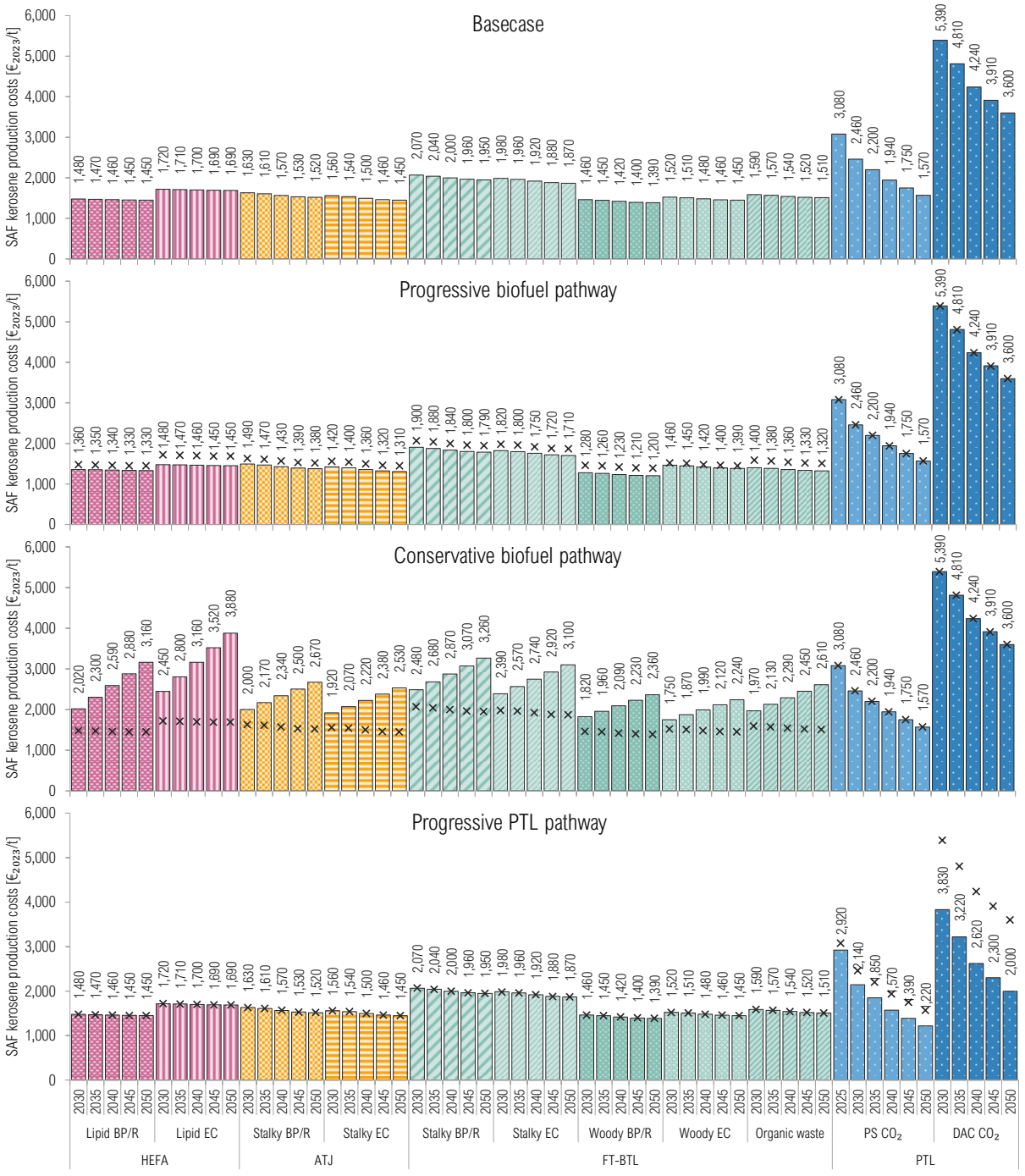

SI Figure 12 SAF kerosene production costs for plant commissioning years 2025 and 2050 across all scenarios (**ATJ**: Alcohol-to-Jet; **BP/R**: by-products and residues; **BTL**: Biomass-to-Liquid; **DAC**: direct-air-capture; **EC**: energy crops; **FT**: Fischer-Tropsch; **HEFA**: Hydroprocessed Esters and Fatty Acids; **PS:** point source; **PTL**: Power-to-Liquid; **WTW**: well-to-wake; the **x** symbols represent the SAF production costs in the basecase scenario as a comparison indication)

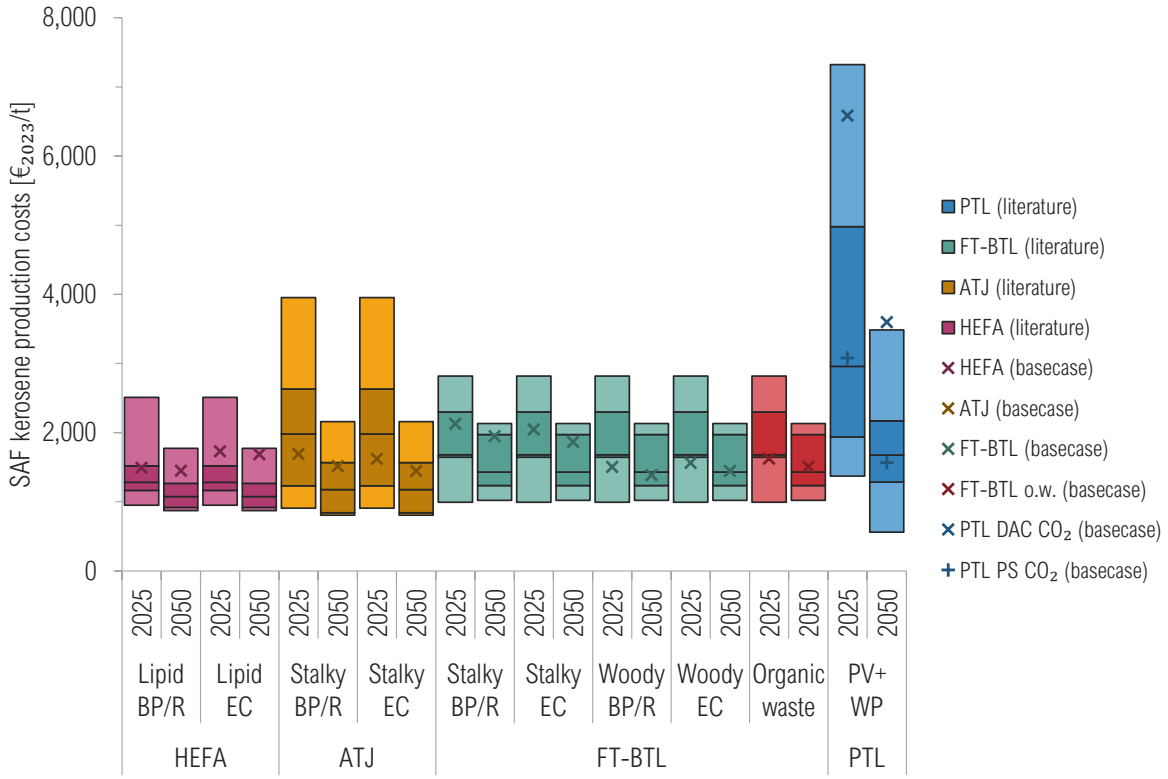

SI Figure 13 SAF kerosene production costs for plant commissioning years 2025 and 2050, presented for the basecase scenario and compared with literature data (**ATJ**: Alcohol-to-Jet; **BP/R**: by-products and residues; **BTL**: Biomass-to-Liquid; **DAC**: direct-air-capture; **EC**: energy crops; **FT**: Fischer-Tropsch; **HEFA**: Hydroprocessed Esters and Fatty Acids; **PS:** point source; **PTL**: Power-to-Liquid; **PV**: photovoltaic; **WP**: wind power; literature data based on [3], [33], [35], [51], [70], [105], [106], [110], [111], [113], [115], [116], [119], [122], [123], [124], [125], [126], [127], [128], [129], [130])

3.6 Fossil Kerosene Price

The price levels for conventional kerosene-based aviation fuels from 2010 to 2024 are shown in SI Figure 14.[4] Since these fuels are primarily produced from crude oil [82], their prices are strongly influenced by global crude oil price levels (SI Figure 15). Market prices for conventional aviation fuels are subject to significant fluctuations. During the period shown in SI Figure 14, aviation fuel prices ranged from approximately €180/t to €1,280/t, with these extremes observed between 2020 and late 2022, potentially as a result of the COVID-19 pandemic. However, aviation fuel prices predominantly ranged between approximately €480/t and €720/t (first to third quartile), aligning with the range of the two-year moving average depicted over time. Across the entire period, the median price was approximately €600/t. Regarding the assumed model input data, it should be noted that the market price of fossil kerosene is strongly influenced by global crude oil price levels and is subject to significant fluctuations (SI Figure 14). A robust estimation of future

[4] The data is based on the U.S. Gulf Coast and does not represent a global average. Price deviations in other regions (e.g., Europe, South America, Asia) are typically within the single-digit percentage range [131] and therefore remain comparable in scale.

market prices is practically impossible. Therefore, a constant kerosene price is assumed in this analysis, based on historical values. A price of 700 €$_{2023}$/t is used, corresponding approximately to the upper value of the 75% percentile of global kerosene prices from 2010 to 2024 (SI Figure 14).

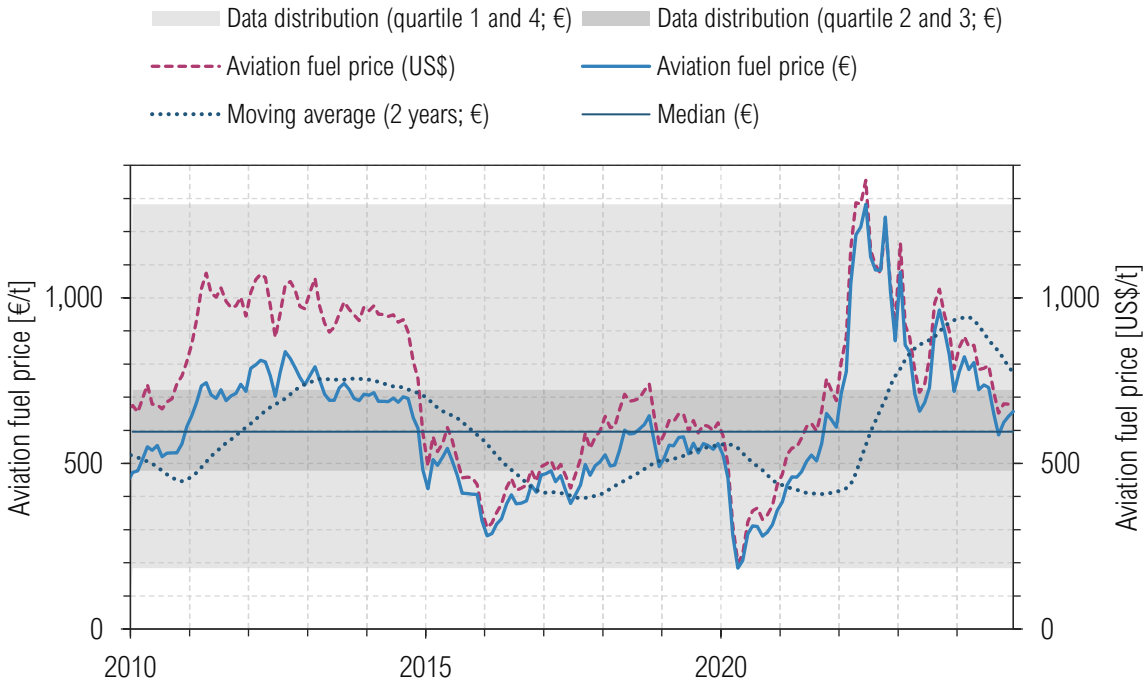

248

249 SI Figure 14 Jet A/A-1 aviation fuel prices from 2010 to 2024 (data source for fuel prices: [72]; data
250 source for exchange rates US$/€: [73])

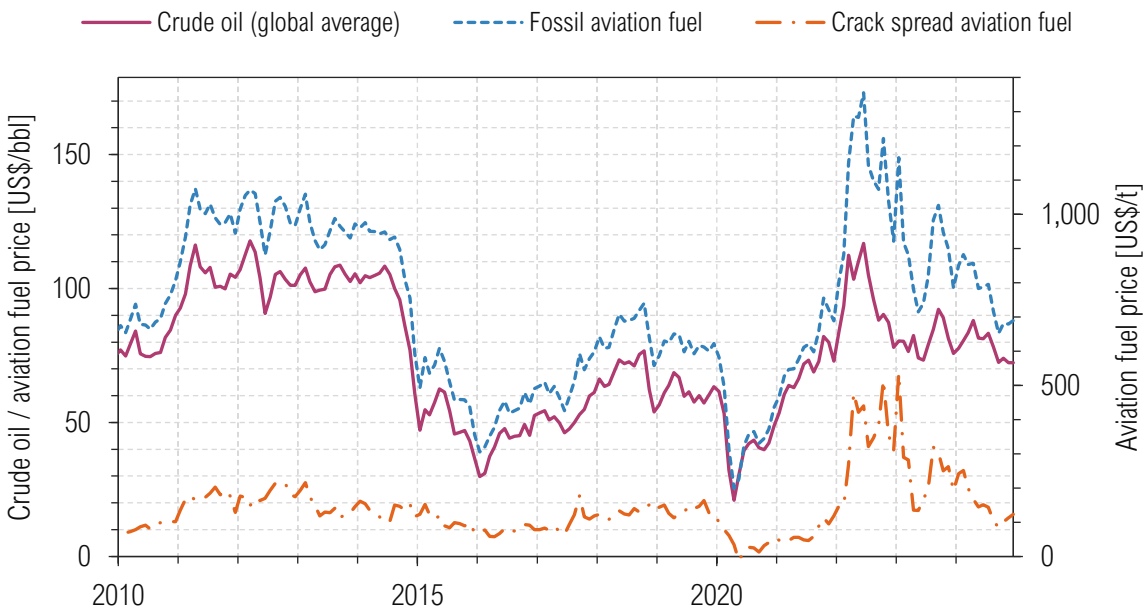

251

252 SI Figure 15 Crude oil prices, Jet A/A-1 aviation fuel prices, and crack spread[5] from 2010 to 2024 (data
253 source for aviation fuel prices: [72]; data source for crude oil prices: [134]).

[5] The so-called "crack spread" refers to the difference between the (purchase) price of crude oil and the (sales) prices of refined petroleum products (e.g., gasoline, kerosene, diesel). It serves as an indicator of the short-term profit margin for refineries [132], [133].

References

[1] Bullerdiek N (2024): Kerosinoptionen auf Basis regenerativer Energien im internationalen Luftverkehr. Dissertation. Technische Universität Hamburg; Verlag Dr. Kovač.

[2] Müller C, Kieckhäfer K, Spengler T S. (2018): The influence of emission thresholds and retrofit options on airline fleet planning: An optimization approach. Energy Policy 112, pp 242–257. DOI: 10.1016/j.enpol.2017.10.022.

[3] Dietrich S, Zech K, Oehmichen K, Müller-Langer F, Majer S, Kalcher J, Naumann K, Wirkner R, Pujan R, Braune M, Gröngröft A, Albrecht U, Raksha T, Weindorf W, Reichmuth M, Gansler J, Schiffler A (2017): Machbarkeitsanalyse für eine PTG-HEFA-Hybridraffinerie in Deutschland. Im Auftrag des Bundesministeriums für Verkehr und digitale Infrastruktur (BMVI) im Rahmen der Mobilitäts- und Kraftstoffstrategie der Bundesregierung (MKS). Deutsches Biomasseforschungszentrum gemeinnützige GmbH (DBFZ); Ludwig-Bölkow-Systemtechnik GmbH (LBST); Leipziger Institut für Energie GmbH (IE-Leipzig). Leipzig.

[4] Vásquez M Cecilia, Silva E Eduardo, Castillo E Fernando (2017): Hydrotreatment of vegetable oils: A review of the technologies and its developments for jet biofuel production. In: Biomass Bioenergy 105:197–206.

[5] Neuling U, Kaltschmitt M (2018): Techno-economic and environmental analysis of aviation biofuels. Fuel Processing Technology. Technische Universität Hamburg (TUHH); Institut für Umwelttechnik und Energiewirtschaft (IUE).

[6] Neuling, U (2019): Biokerosinherstellung. Verfahrensidentifikation, Simulation und Bewertung. 1. Auflage. Hamburg: Kovac, Dr. Verlag (Schriftenreihe Technische Forschungsergebnisse, 34).

[7] Laveille P, Uratani J, Barron J G. G., Brodeur-Campbell M, Chandak N R., George A, Morin S, Galvan A R., Berthod M (2022): Sustainable pilot-scale production of a Salicornia oil, its conversion to certified aviation fuel, and techno-economic analysis of the related biorefinery. Biofuels, Bioproducts and Biorefining 16 (1), pp 27–42. DOI: 10.1002/bbb.2260.

[8] Kaltschmitt M, Müller-Langer F, Neuling U, Remmele E, Thuneke K (2016): Produktion und Nutzung von Pflanzenölkraftstoffen. In: Martin Kaltschmitt, Hans Hartmann und Hermann Hofbauer (eds.): Energie aus Biomasse. 3., aktualisierte Aufl. 2016. Berlin, Heidelberg: Springer Berlin Heidelberg; Imprint: Springer Vieweg, pp 1339–1445.

[9] IEA (2021): Progress in Commercialization of Biojet/Sustainable Aviation Fuels (SAF): Technologies, potential and challenges. IEA Bioenergy Task 39. International Energy Agency (IEA). Paris.

[10] Lewandowski I (2016): Landwirtschaftlich produzierte Biomasse. In: Martin Kaltschmitt, Hans Hartmann und Hermann Hofbauer (eds.): Energie aus Biomasse. 3., aktualisierte Aufl. 2016. Berlin, Heidelberg: Springer Berlin Heidelberg; Imprint: Springer Vieweg, pp 167–247.

[11] Friedl A, Miltner A, Neuling U, Kaltschmitt M (2016): Fermentative Alkoholerzeugung und -nutzung. In: Martin Kaltschmitt, Hans Hartmann und Hermann Hofbauer (eds.): Energie aus Biomasse. 3., aktualisierte Aufl. 2016. Berlin, Heidelberg: Springer Berlin Heidelberg; Imprint: Springer Vieweg, pp 1501–1607.

[12] Tao L, Markham J N., Haq Z, Biddy M J. (2017): Techno-economic analysis for upgrading the biomass-derived ethanol-to-jet blendstocks. Green Chemistry 19 (4), pp 1082–1101. DOI: 10.1039/c6gc02800d.

[13] CAAFI (2023): Fuel Qualification. Approved Fuels. Commercial Aviation Alternative Fuels Initiative (CAAFI). URL: www.caafi.org/focus_areas/fuel_qualification.html. Accessed 17 Aug 2023.

[14] van Dyk S, Saddler J (2024): Progress in Commercialization of Biojet/Sustainable Aviation Fuels (SAF): Technologies and policies. IEA Bioenergy Task 39. International Energy Agency (IEA). Paris.

[15] Schemme S (2020): Techno-ökonomische Bewertung von Verfahren zur Herstellung von Kraftstoffen aus H2 und CO2. Dissertation. RWTH Aachen. Aachen.
[16] Kuhz H (2015): Konversion von Ethanol zu Butanol an heterogenen Katalysatoren. Dissertation. Technische Universität Carolo-Wilhelmina zu Braunschweig. Braunschweig. Accessed 07 Nov 2021.
[17] Hofbauer H, Kaltschmitt M, Keil F, Neuling U, Wagner H (2016): Vergasung in der Gasatmosphäre. In: Martin Kaltschmitt, Hans Hartmann und Hermann Hofbauer (eds.): Energie aus Biomasse. 3., aktualisierte Aufl. 2016. Berlin, Heidelberg: Springer Berlin Heidelberg; Imprint: Springer Vieweg, pp 1059–1182.
[18] Dürre P, Eikmanns B J. (2015): C1-carbon sources for chemical and fuel production by microbial gas fermentation. Current opinion in biotechnology 35, pp 63–72. DOI: 10.1016/j.copbio.2015.03.008.
[19] Stoll I Katharina, Boukis N, Sauer J (2020): Syngas Fermentation to Alcohols: Reactor Technology and Application Perspective. Chemie Ingenieur Technik 92 (1-2), pp 125–136. DOI: 10.1002/cite.201900118.
[20] Müller-Langer F (2011): Analyse und Bewertung ausgewählter zukünftiger Biokraftstoffoptionen auf der Basis fester Biomasse. DBFZ Report Nr. 9. Dissertation. Deutsches Biomasseforschungszentrum gemeinnützige GmbH (DBFZ). Leipzig.
[21] Arshad M, Abbas M, Javed S, Adil M, Shahzad M Imran, Iqbal M (2021): Sustainable Ethanol Production: An Overview. In: Muhammad Arshad (ed.): Sustainable Ethanol and Climate Change. Sustainability Assessment for Ethanol Distilleries. 1st ed. 2021. Cham: Springer International Publishing; Imprint: Springer, pp 1–14.
[22] Pechstein J, Gebauer J, Neuling U, Kaltschmitt M (2015): Biokerosin aus Alkoholen. Substrate, Konzepte und Verfahren, Bewertung. Abschlussbericht. Institut für Umwelttechnik und Energiewirtschaft (IUE). Hamburg.
[23] Harsche J, Herrmann R, Honermeier B (2014): Agrarische Rohstoffe – Stoffströme, gesamtwirtschaftliche Bewertung und soziale Akzeptanz. In: Jörg Böttcher, Nina Hampl, Martin Kügemann und Florian Lüdeke-Freund (eds.): Biokraftstoffe und Biokraftstoffprojekte. Rechtliche, technische und wirtschaftliche Aspekte: Springer Berlin Heidelberg, pp 185–212.
[24] Romero-Izquierdo A Guadalupe, Gómez-Castro F Israel, Gutiérrez-Antonio C, Hernández S, Errico M (2021): Intensification of the alcohol-to-jet process to produce renewable aviation fuel. Chemical Engineering and Processing - Process Intensification 160, p 108270. DOI: 10.1016/j.cep.2020.108270.
[25] Geleynse S, Brandt K, Garcia-Perez M, Wolcott M, Zhang X (2018): The Alcohol-to-Jet Conversion Pathway for Drop-In Biofuels: Techno-Economic Evaluation. ChemSusChem 11 (21), pp 3728–3741. DOI: 10.1002/cssc.201801690.
[26] Bullerdiek N, Voß S, Neuling U, Kaltschmitt M (2022): Direct alcohol vs. alcohol-to-jet SPK utilisation in commercial aviation - an energetic-operational analysis. International Journal of Sustainable Aviation 8 (3), p 1. DOI: 10.1504/IJSA.2022.10046511.
[27] Eagan N M., Kumbhalkar M D., Buchanan J Scott, Dumesic J A., Huber G W. (2019): Chemistries and processes for the conversion of ethanol into middle-distillate fuels. Nature Reviews Chemistry 3 (4), pp 223–249. DOI: 10.1038/s41570-019-0084-4.
[28] Coker, A Kayode (2018): Petroleum Refining Designs and Applications Handbook. Somerset: John Wiley & Sons Incorporated.
[29] Pechstein J, Zschocke A (2018): Blending of Synthetic Kerosene and Conventional Kerosene. In: Martin Kaltschmitt und Ulf Neuling (eds.): Biokerosene. Status and prospects. Berlin: Springer, pp 665–686.
[30] Klerk, A de (2011): Fischer-Tropsch refining. Weinheim: WILEY-VCH.
[31] Mesfun S Asmelash (2022): Biomass to Liquids (BtL) via Fischer-Tropsch. A brief review. Prepared with the support of project ETIP-B-SABS2. European Technology and Innovation

Platform (ETIP). URL: https://www.etipbioenergy.eu/images/ETIP_B_Factsheet_BtL_2021.pdf.
[32] Meurer A, Kern J (2021): Fischer–Tropsch Synthesis as the Key for Decentralized Sustainable Kerosene Production. Energies 14 (7), p 1836. DOI: 10.3390/en14071836.
[33] Batteiger V, Ebner K, Habersetzer A, Moser L, Weindorf W, Raksha T (2022): Power-to-Liquids. A scalable and sustainable fuel supply perspective for aviation. Umweltbundesamt (UBA); Bauhaus Luftfahrt e. V. (BHL); Ludwig-Bölkow-Systemtechnik GmbH (LBST). Dessau-Roßlau.
[34] Sizmann A (2016): Solar-Jet. Project Final Report. Bauhaus Luftfahrt e. V. (BHL). Ottobrun.
[35] CST, WEF (2020): Sustainable Aviation Fuels as a Pathway to Net-Zero Aviation. Insight Report. Clean Skies for Tomorrow (CST); McKinsey & Company; World Economic Forum (WEF). Genf.
[36] Jack M W. (2009): Scaling laws and technology development strategies for biorefineries and bioenergy plants. Bioresource technology 100 (24), pp 6324–6330. DOI: 10.1016/j.biortech.2009.06.109.
[37] Michailos S, Bridgwater A (2019): A comparative techno-economic assessment of three bio-oil upgrading routes for aviation biofuel production. International Journal of Energy Research. DOI: 10.1002/er.4745.
[38] Searcy E, Flynn P (2009): The impact of biomass availability and processing cost on optimum size and processing technology selection. Applied biochemistry and biotechnology 154 (1-3), pp 92–107. DOI: 10.1007/s12010-008-8407-9.
[39] Wright M, Brown R C. (2007): Establishing the optimal sizes of different kinds of biorefineries. Biofuels, Bioproducts and Biorefining 1 (3), pp 191–200. DOI: 10.1002/bbb.25.
[40] Leboreiro J, Hilaly A K. (2011): Biomass transportation model and optimum plant size for the production of ethanol. Bioresource technology 102 (3), pp 2712–2723. DOI: 10.1016/j.biortech.2010.10.144.
[41] Daugaard T, Mutti L A., Wright M M., Brown R C., Componation P (2015): Learning rates and their impacts on the optimal capacities and production costs of biorefineries. Biofuels, Bioproducts and Biorefining 9 (1), pp 82–94. DOI: 10.1002/bbb.1513.
[42] Dieckmann C, Edelmann W, Kaltschmitt M, Liebetrau J, Oldenburg S, Ritzkowski M, Scholwin F, Sträuber H, Weinrich S (2016): Biogaserzeugung und -nutzung. In: Martin Kaltschmitt, Hans Hartmann und Hermann Hofbauer (eds.): Energie aus Biomasse. 3., aktualisierte Aufl. 2016. Berlin, Heidelberg: Springer Berlin Heidelberg; Imprint: Springer Vieweg, pp 1609–1755.
[43] Klerk A de (Hg.) (2013): Greener Fischer-Tropsch processes for fuels and feedstocks. Weinheim: WILEY-VCH.
[44] Ostadi M, Rytter E, Hillestad M (2019): Boosting carbon efficiency of the biomass to liquid process with hydrogen from power: The effect of H2/CO ratio to the Fischer-Tropsch reactors on the production and power consumption. Biomass and Bioenergy 127, p 105282. DOI: 10.1016/j.biombioe.2019.105282.
[45] Rauch R, Hofbauer H, Neuling U, Kaltschmitt M (2018): Biokerosene Production from Bio-Chemical and Thermo-Chemical Biomass Conversion and Subsequent Fischer-Tropsch Synthesis. In: Martin Kaltschmitt und Ulf Neuling (eds.): Biokerosene. Status and prospects. Berlin: Springer, pp 497–542.
[46] König H (2016): Techno-ökonomische Prozessbewertung der Herstellung synthetischen Flugturbinentreibstoffes aus CO2 und H2. Dissertation. Universität Stuttgart. Stuttgart.
[47] Behr, A, Agar, D W., Jörissen, J, Vorholt, A J. (2016): Einführung in die Technische Chemie. 2. Auflage. Berlin: Springer Spektrum (Lehrbuch).
[48] Hsu C Samuel, Robinson P R. (Hg.) (2017): Springer handbook of petroleum technology. With 754 figures and 282 Tables. Cham: Springer International Publishing (Springer Handbooks).

[49] Zschocke A, Scheuermann S, Ortner J (2017): High Biofuel Blends in Aviation (HBBA). ENER/C2/2012/ 420-1. Final Report. Deutsche Lufthansa AG; Wehrwissenschaftliches Institut für Werk- und Betriebsstoffe (WIWEB). Frankfurt am Main, Koblenz.
[50] Bube S, Bullerdiek N, Voß S, Kaltschmitt M (2024): Kerosene production from power-based syngas – A technical comparison of the Fischer-Tropsch and methanol pathway. Fuel 366, p 131269. DOI: 10.1016/j.fuel.2024.131269.
[51] Brynolf S, Taljegard M, Grahn M, Hansson J (2018): Electrofuels for the transport sector: A review of production costs. Renewable and Sustainable Energy Reviews. Rev 81: 1887–1905.
[52] Diekmann B, Rosenthal E (Hg.) (2014): Energie. Physikalische Grundlagen ihrer Erzeugung, Umwandlung und Nutzung. 3., vollst. überarb. und erw. Aufl. Wiesbaden: Springer Spektrum.
[53] Sterner, M, Stadler, I (2018): Handbook of Energy Storage. Demand, Technologies, Integration. Berlin, s.l.: Springer Berlin.
[54] Dieterich V, Buttler A, Hanel A, Spliethoff H, Fendt S (2020): Power-to-liquid via synthesis of methanol, DME or Fischer–Tropsch-fuels: a review. Energy Environ. Sci. 13 (10), pp 3207–3252. DOI: 10.1039/d0ee01187h.
[55] IEA (2021): Global Hydrogen Review. International Energy Agency (IEA). Paris.
[56] Sterner, M, Stadler, I (2016): Energiespeicher - Bedarf, Technologien, Integration. Berlin, Heidelberg: Springer Berlin Heidelberg.
[57] Adelung S, Dietrich R-U (2022): Impact of the reverse water-gas shift operating conditions on the Power-to-Liquid fuel production cost. Fuel 317, p 123440. DOI: 10.1016/j.fuel.2022.123440.
[58] Fröhlich T, Blömer S, Münter D, Brischke L-A (2019): CO2-Quellen für die PtX-Herstellung in Deutschland - Technologien, Umweltwirkung, Verfügbarkeit. ifeu paper 03/2019. Heidelberg.
[59] Marchese M, Buffo G, Santarelli M, Lanzini A (2021): CO2 from direct air capture as carbon feedstock for Fischer-Tropsch chemicals and fuels: Energy and economic analysis. Journal of CO2 Utilization 46, p 101487. DOI: 10.1016/j.jcou.2021.101487.
[60] Fasihi M, Efimova O, Breyer C (2019): Techno-economic assessment of CO2 direct air capture plants. Journal of Cleaner Production 224, pp 957–980. DOI: 10.1016/j.jclepro.2019.03.086.
[61] González-Castaño M, Dorneanu B, Arellano-García H (2021): The reverse water gas shift reaction: a process systems engineering perspective. Reaction Chemistry & Engineering 6 (6), pp 954–976. DOI: 10.1039/d0re00478b.
[62] IEA (2023): ETP Clean Energy Technology Guide – Data Tools - IEA. International Energy Agency (IEA). Paris. URL: https://www.iea.org/data-and-statistics/data-tools/etp-clean-energy-technology-guide?search=reverse+water, zuletzt aktualisiert am 3/20/2023. Accessed 20 Mar 2023.
[63] Wenzel M (2018): Reverse water-gas shift chemical looping for syngas production from CO2. Dissertation. Otto-von-Guericke-Universität Magdeburg. Magdeburg.
[64] Rezaei E, Dzuryk S (2019): Techno-economic comparison of reverse water gas shift reaction to steam and dry methane reforming reactions for syngas production. Chemical Engineering Research and Design 144, pp 354–369. DOI: 10.1016/j.cherd.2019.02.005.
[65] Bube S, Voß S, Quante G, Kaltschmitt M (2025): Cost analysis of kerosene production from power-based syngas via the Fischer-Tropsch and methanol pathway. Fuel 384, p 133901. DOI: 10.1016/j.fuel.2024.133901.
[66] Sens L, Piguel Y, Neuling U, Timmerberg S, Wilbrand K, Kaltschmitt M (2022): Cost minimized hydrogen from solar and wind – Production and supply in the European catchment area. Energy Conversion and Management 265, p 115742. DOI: 10.1016/j.enconman.2022.115742.
[67] SkyNRG (2024): Sustainable Aviation Fuel Market Outlook 2024. June 2024 Update. SkyNRG. URL: https://www.efuel-alliance.eu/fileadmin/Downloads/SAF-Market-Outlook-2024-Summary.pdf. Accessed 22 Jan 2025.

[68] Argus (2023): Global SAF capacity map 2023 (Update XIII). Argus Media group. URL: https://view.argusmedia.com/Global_SAF_Capacity_Map.html.
[69] Jong S de, Hoefnagels R, Faaji A, Slade R, Mawhood R, Junginger H Martin (2015): The feasibility of short-term production strategies for renewable jet fuels – a comprehensive techno-economic comparison (6).
[70] Pavlenko N, Searle S, Christensen A (2019): The cost of supporting alternative jet fuels in the European Union. International Council on Clean Transportation (ICCT). Wilmington. Accessed 15 May 2019.
[71] IATA (2019): An Airline Handbook on CORSIA. International Air Transport Association (IATA). Montréal.
[72] EIA (2025): U.S. Gulf Coast Kerosene-Type Jet Fuel Spot Price FOB (Dollars per Gallon). U.S. Energy Information Administration (EIA). URL: https://www.eia.gov/dnav/pet/hist/LeafHandler.ashx?n=PET&s=EER_EPJK_PF4_RGC_DPG&f=M. Accessed 22 Jan 2025.
[73] ECB (2025): ECB Statistical Data Warehouse. ECB Reference Exchange Rate, US Dollar/Euro. European Central Bank (ECB). Brüssel. URL: http://sdw.ecb.europa.eu/quickview.do?org.apache.struts.taglib.html.TOKEN=c405ab7972b7b18804c026ccad802c0c&SERIES_KEY=120.EXR.D.USD.EUR.SP00.A&start=01-01-2009&end=26-07-2019&submitOptions.x=0&submitOptions.y=0&trans=N. Accessed 22 Jan 2025.
[74] UNDP (2022): Report on CORSIA implications and carbon market development (Deliverable 3.2.). United Nations Development Programme (UNDP).
[75] Towler, G, Sinnott, R K. (2012): Chemical engineering design. Principles, practice, and economics of plant and process design. Second edition. Amsterdam: Elsevier.
[76] IATA (2024): Industry Statistics End-year. Fact Sheet. International Air Transport Association (IATA). Montréal.
[77] ATAG (2021): Waypoint 2050. Second Edition. Balancing growth in connectivity with a comprehensive global air transport response to the climate emergency: a vision of net-zero aviation by mid-century. Air Transport Action Group (ATAG). Genf.
[78] ICAO (2021): Post-COVID-19 Forecasts Scenarios. COVID-19 Impact on the ICAO Long-Term Traffic Forecasts. Appendix A: Traffic Forecasts. International Civil Aviation Organization (ICAO). Montréal.
[79] Dray L, Schäfer A W., Grobler C, Falter C, Allroggen F, Stettler M E. J., Barrett S R. H. (2022): Cost and emissions pathways towards net-zero climate impacts in aviation. Nature Climate Change 12 (10), pp 956–962. DOI: 10.1038/s41558-022-01485-4.
[80] ICAO (2022): Resolution A41-21. Consolidated statement of continuing ICAO policies and practices related to environmental protection - Climate change. International Civil Aviation Organization (ICAO). Montréal.
[81] ICAO (2010): Resolution A37-19: Consolidated statement of continuing ICAO policies and practices related to environmental protection - Climate change. International Civil Aviation Organization (ICAO). Montréal.
[82] ICAO (2022): Environmental Report 2022. International Civil Aviation Organization (ICAO). Montréal.
[83] IATA (2018): Industry Forecast Mid-year. Economic Performance of the Airline Industry. June 2018. International Air Transport Association (IATA). Montréal.
[84] IATA (2019): Industry Statistics Mid-year. Fact Sheet. June 2019. International Air Transport Association (IATA). Montréal.
[85] IATA (2019): Industry Statistics End-year. Fact Sheet. December 2019. International Air Transport Association (IATA). Montréal.
[86] IATA (2021): Industry Statistics Mid-year. Fact Sheet. April 2021. International Air Transport Association (IATA). Montréal.

[87] IATA (2021): Industry Statistics End-year. Fact Sheet. October 2021. International Air Transport Association (IATA). Montréal.
[88] IATA (2022): Industry Statistics Mid-year. Fact Sheet. June 2022. International Air Transport Association (IATA). Montréal.
[89] IATA (2022): Industry Statistics End-year. Fact Sheet. December 2022. International Air Transport Association (IATA). Montréal.
[90] IATA (2023): Industry Statistics Mid-year. Fact Sheet. International Air Transport Association (IATA). Montréal.
[91] Kaltschmitt M, Sens L, Streicher W (2020): Einführung und Aufbau. In: Martin Kaltschmitt, Wolfgang Streicher und Andreas Wiese (eds.): Erneuerbare Energien. Systemtechnik, Wirtschaftlichkeit, Umweltaspekte. 6., vollständig neu überarbeitete Auflage. Berlin, Heidelberg: Springer Vieweg, pp 3–58.
[92] Bloche-Daub K, Hartmann H, Hofbauer H, Kaltschmitt M, Pfeiffer D, Thormann L, Thrän D (2016): Einleitung und Zielsetzung. In: Martin Kaltschmitt, Hans Hartmann und Hermann Hofbauer (eds.): Energie aus Biomasse. 3., aktualisierte Aufl. 2016. Berlin, Heidelberg: Springer Berlin Heidelberg; Imprint: Springer Vieweg, pp 1–76.
[93] IEA (2017): Technology Roadmap. Delivering Sustainable Bioenergy. International Energy Agency (IEA). Paris.
[94] ETC (2021): Bioresources within a Net-Zero Emissions Economy: Making a Sustainable Approach Possible. Version 1.0. Energy Transitions Commission (ETC).
[95] IRENA (2022): World Energy Transitions Outlook 2022. 1.5°C Pathway. International Renewable Energy Agency (IRENA). Abu Dhabi.
[96] Thrän D, Cowie A, Berndes G (2020): Roles of bioenergy in energy system pathways towards a "well-below-2-degrees-Celsius (WB2)" world. Workshop report and synthesis of presented studies. IEA Bioenergy: International Energy Agency (IEA). Paris.
[97] CCC (2018): Biomass in a low-carbon economy. Committee on Climate Change (CCC). London.
[98] IEA (2022): World Energy Outlook 2022. International Energy Agency (IEA). Paris.
[99] Shell (2017): Global Energy Resources database. Shell Global. URL: https://www.shell.com/energy-and-innovation/the-energy-future/scenarios/shell-scenarios-energy-models/energy-resource-database.html#iframe=L3dlYmFwcHMvRW5lcmd5UmVzb3VyY2VEYXRhYmFzZS8jY2xvc2U, zuletzt aktualisiert am 12/11/2022. Accessed 11 Dec 2022.
[100] Searle S, Malins C (2015): A reassessment of global bioenergy potential in 2050. GCB Bioenergy 7 (2), pp 328–336. DOI: 10.1111/gcbb.12141.
[101] WBGU (2008): Welt im Wandel. Zukunftsfähige Bioenergie und nachhaltige Landnutzung. Wissenschaftlicher Beirat der Bundesregierung Globale Umweltveränderungen (WGBU). Berlin. URL: https://www.wbgu.de/de/publikationen/publikation/welt-im-wandel-zukunftsfaehige-bioenergie-und-nachhaltige-landnutzung#sektion-downloads.
[102] Strengers B, Elzenga H (2020): Availability and applications of sustainable biomass. Report on a search for shared facts and views. Netherlands Environmental Assessment Agency (PBL). Den Haag.
[103] Haberl H, Beringer T, Bhattacharya S C., Erb K-H, Hoogwijk M (2010): The global technical potential of bio-energy in 2050 considering sustainability constraints. Current opinion in environmental sustainability 2 (5-6), pp 394–403. DOI: 10.1016/j.cosust.2010.10.007.
[104] IEA Bioenergy (2007): Potential Contribution of Bioenergy to the World's Future Energy Demand. International Energy Agency (IEA). Paris. URL: https://www.ieabioenergy.com/wp-content/uploads/2013/10/Potential-Contribution-of-Bioenergy-to-the-Worlds-Future-Energy-Demand.pdf. Accessed 28 Nov 2021.
[105] MPP (2022): Making Net-Zero Aviation Possible. An industry-backed, 1.5°C-aligned transition strategy. Mission Possible Partnership (MPP).

[106] ICF (2021): Fueling Net Zero. How the aviation industry can deploy sufficient sustainable aviation fuel to meet climate ambitions. An ICF Report for ATAG Waypoint 2050. ICF International.

[107] SkyNRG (2021): SAF Market Outlook. SkyNRG's Perspective on the ReFuelEU Aviation initiative Proposal. Background Analysis. SkyNRG. Amsterdam.

[108] Dray L, Schäfer A W., Grobler C, Falter C, Allroggen F, Stettler M E. J., Barrett S R. H. (2022): Cost and emissions pathways towards net-zero climate impacts in aviation. Supplementary Information (10).

[109] IRENA (2023): Renewable Capacity Statistics 2023. IRENASTAT Online Data Query Tool. Installed renewable electricity capacity (MW) by Region/country/area, Technology and Year. International Renewable Energy Agency (IRENA). URL: https://pxweb.irena.org/pxweb/en/IRENASTAT/IRENASTAT__Power%20Capacity%20and%20Generation/RECAP_2023_cycle2.px/, zuletzt aktualisiert am 8/4/2023. Accessed 04 Aug 2023.

[110] Neuling U, Kaltschmitt M (2019): Aviation biofuels: an economic and environmental assessment with an outlook on cost reduction potentials. International Conference on Polygeneration Strategies ICPS19. Hamburg University of Technology (TUHH); Institute of Environmental Technology and Energy Economics (IUE). Wien.

[111] Schmidt P, Weindorf W, Roth A, Batteiger V, Riegel F (2016): Power-to-Liquids. Potentials and Perspectives for the Future Supply of Renewable Aviation Fuel. Hg. v. Umweltbundesamt (UBA). Ludwig-Bölkow-Systemtechnik GmbH (LBST); Bauhaus Luftfahrt e.V. Dessau-Roßlau.

[112] Staples M D., Malina R, Suresh P, Hileman J I., Barrett S R.H. (2018): Aviation CO2 emissions reductions from the use of alternative jet fuels. Energy Policy 114, pp 342–354. DOI: 10.1016/j.enpol.2017.12.007.

[113] Staples M D., Malina R, Olcay H, Pearlson M N., Hileman J I., Boies A, Barrett S R. H. (2014): Lifecycle greenhouse gas footprint and minimum selling price of renewable diesel and jet fuel from fermentation and advanced fermentation production technologies. Energy Environ. Sci. 7 (5), pp 1545–1554. DOI: 10.1039/c3ee43655a.

[114] Brooks K P., Snowden-Swan L J., Jones S B., Butcher M G., Lee G-S, Anderson D M., Frye J G., Holladay J E., Owen J, Harmon L, Burton F, Palou-Rivera I, Plaza J, Handler R, Shonnard D (2016): Low-Carbon Aviation Fuel Through the Alcohol to Jet Pathway. In: Christopher J. Chuck (ed.): Biofuels for Aviation: Elsevier, pp 109–150.

[115] Zech K, Naumann K, Müller-Langer F, Ponitka J, Majer S, Schmidt P, Weindorf W, Altmann M, Michalski J, Niklaß M, Meyer H, Lischke A, Fehrenbach H, Jöhrens J, Markwardt S (2016): Biokerosin und EE-Kerosin für die Luftfahrt der Zukunft – von der Theorie zu Pilotvorhaben. Studie im Rahmen des Auftrags Wissenschaftliche Begleitung, Unterstützung und Beratung des BMVI in den Bereichen Verkehr und Mobilität mit besonderem Fokus auf Kraftstoffe und Antriebstechnologien sowie Energie und Klima für das Bundesministerium für Verkehr und digitale Infrastruktur (BMVI). Deutsches Zentrum für Luft- und Raumfahrt e. V. (DLR); Institut für Energie- und Umweltforschung Heidelberg GmbH (ifeu); Ludwig-Bölkow-Systemtechnik GmbH (LBST); Deutsches Biomasseforschungszentrum gemeinnützige GmbH (DBFZ). Leipzig, München, Berlin, Heidelberg.

[116] Fagerström A, Grahn D, Lundberg S, Ghosh S, Creaser D, Olsson L, Abdelaziz O, Wallberg O, Hulteberg C, Poulikidou S, Lewrén A, Rydberg T, Martin M, Anderson S, Hansson J, Hjort A (2021): Large scale bio electro jet fuel production integration at CHP-plant in Östersund, Sweden. Report number: B 2407. IVL Swedish Environmental Research Institute Ltd.

[117] Han J, Elgowainy A, Cai H, Wang M Q. (2013): Life-cycle analysis of bio-based aviation fuels. Bioresource technology 150, pp 447–456. DOI: 10.1016/j.biortech.2013.07.153.

[118] Zemanek D, Champagne P, Mabee W (2020): Review of life-cycle greenhouse-gas emissions assessments of hydroprocessed renewable fuel (HEFA) from oilseeds. Biofuels, Bioproducts and Biorefining 14 (5), pp 935–949. DOI: 10.1002/bbb.2125.

[119] Zschocke A (2014): Abschlussbericht zu dem Vorhaben Projekt BurnFAIR. Arbeitspakete 1.1 bis 1.4. Deutsche Lufthansa AG. Köln.

[120] ICAO (2019): CORSIA Eligible Fuels – Life Cycle Assessment Methodology. International Civil Aviation Organization (ICAO). Montréal.

[121] Bullerdiek N, Dögnitz N, Kaltschmitt M, Majer S, Müller-Langer F, Neuling U, Oehmichen K (2019): Lebenszyklusanalysen für die eingesetzten SPK und Multiblend JET A-1. Interne Dokumentation. Forschungs- und Demonstrationsvorhaben zum Einsatz von erneuerbarem Kerosin am Flughafen Leipzig / Halle (DEMO-SPK). Technische Universität Hamburg (TUHH); Deutsches Biomasseforschungszentrum gemeinnützige GmbH (DBFZ). Hamburg, Leipzig.

[122] Jong S de (2018): Green Horizons. On the production costs, climate impact and future supply of renewable jet fuels. PhD thesis. Universität Utrecht. Utrecht.

[123] EC (2021): Proposal for a regulation of the European Parliament and of the council on ensuring a level playing field for sustainable air transport. Document 52021PC0561. European Commission (EC). Brussels.

[124] Frontier Economics (2021): Wirtschaftlichkeit von PtX-Produkten aus Nordafrika – Business Case Analysen. Frontier Economics Ltd.

[125] Agora Verkehrswende, Agora Energiewende, Frontier Economics Ltd. (2018): Die zukünftigen Kosten strombasierter synthetischer Brennstoffe. Schlussfolgerungen aus Sicht von Agora Verkehrswende und Agora Energiewende. Frontier Economics Ltd. Berlin.

[126] Schmidt P, Zittel W, Weindorf W, Raksha T (2016): Renewables in Transport 2050. Empowering a sustainable mobility future with zero emission fuels from renewable electricity. Kraftstoffstudie II. Final Report. Forschungsvereinigung Verbrennungskraftmaschinen (FVV) e.V. Frankfurt am Main.

[127] Fasihi M, Bogdanov D, Breyer C (2016): Techno-Economic Assessment of Power-to-Liquids (PtL) Fuels Production and Global Trading Based on Hybrid PV-Wind Power Plants. Energy Procedia 99, pp 243–268. DOI: 10.1016/j.egypro.2016.10.115.

[128] Pfennig M, Bonin M von, Gerhardt N (2021): PtX-Atlas: Weltweite Potenziale für die Erzeugung von grünem Wasserstoff und klimaneutralen synthetischen Kraft- und Brennstoffen. Teilbericht im Rahmen des Projektes: DeV-KopSys. PTX-ATLAS Hintergrundpapier. Fraunhofer-Institut für Energiewirtschaft und Energiesystemtechnik (Fraunhofer IEE).

[129] Pfennig M, Gerhardt N, Pape C, Böttger D (2017): Mittel- und langfristige Potenziale von PtL- und H2-Importen aus internationalen EE-Vorzugsregionen. Teilbericht. Fraunhofer IWES).

[130] König D H., Albrecht F G., Dietrich R-U (2016): Power and Biomass-to-Liquid (PBtL): a Promising Approach to Produce Biofuels using Electricity. Hg. v. ETA-Florence Renewable Energies.

[131] IATA (2023): Jet Fuel Price Monitor. International Air Transport Association (IATA). Montréal. URL: https://www.iata.org/publications/economics/fuel-monitor/Pages/index.aspx. Accessed 04 Jan 2023.

[132] EIA (2013): Crack Spread. U.S. Energy Information Administration (EIA). Washington D.C. URL: https://www.eia.gov/todayinenergy/includes/crackspread_explain.php. Accessed 23 Oct 2019.

[133] Hileman J I., Stratton R W. (2014): Alternative jet fuel feasibility. Transport Policy 34, pp 52–62. DOI: 10.1016/j.tranpol.2014.02.018.

[134] World Bank (2025): Commodity Markets. Monthly prices. Februar 2023. World Bank. Washington D.C. URL: http://pubdocs.worldbank.org/en/561011486076393416/CMO-Historical-Data-Monthly.xlsx, zuletzt aktualisiert am 1/22/2025. Accessed 22 Jan 2025.